Investigation on the dynamic behaviors of the coupled memcapacitor-based circuits*

Zhi Zhou(周知)[1], Dong-Sheng Yu(于东升)[1,†], and Xiao-Yuan Wang(王晓媛)[2]

[1] School of Electrical and Power Engineering, China University of Minning and Technology, Xuzhou 221116, China

[2] School of Electronic Information, Hangzhou Dianzi University, Hangzhou 310018, China

(Received 17 July 2017; revised manuscript received 16 August 2017; published online 20 October 2017)

In this paper, by referring to the concept of coupled memristors (MRs) and considering the flux coupling connection, the constitutive relations for describing the coupled memcapacitors (MCs) are theoretically deduced. The dynamic behaviors of dual coupled MCs in serial and parallel connections are analyzed in terms of identical or opposite polarities for the first time. Based on the derived constitutive relations of the two coupled MCs, the modified relaxation oscillators (ROs) are obtained with the purpose of achieving controllable oscillation frequency and duty cycle. In consideration of different parameter configurations, the experimental investigation is carried out by using practical off-the-shelf circuit components to verify the correction of the theoretical calculation with numerical simulation of the coupled MCs and its application in ROs.

Keywords: memcapacitor, coupling strength, relaxation oscillator, parallel/serial connection

PACS: 07.50.Ek, 84.30.Ng, 85.25.Hv **DOI:** 10.1088/1674-1056/26/12/120701

1. Introduction

In 1971, the fourth fundamental circuit element called memristor (MR) was originally speculated by Chua as a two-terminal nonlinear passive component which is capable of memorizing the amount of historic charge passing through it.[1] In 2009, by taking an extra step, the concept of memory devices was generalized to capacitor and another hypothetical mem-elements called memcapacitor (MC) was conceptually proposed in Ref. [2]. A generalized MR consisting of a memristive diode bridge with the first-order RC filter in parallel connection was discussed in Ref. [3]. By introducing also a generalized MR and an LC absorbing network into Wien-bridge oscillator, a new memristive Wien-bridge chaotic oscillator was designed and analyzed in Ref. [4]. In Ref. [5], a physical memristive device was newly discussed, whose ionic drift direction is perpendicular to the direction of the applied voltage, and then a novel threshold flux-controlled MR model with a window function was proposed. Compared with the MRs, MCs are capable of storing energy in addition to information, and hence could explore new orientations in the important technological area of energy storage and circuit operation. Up to now, tremendous efforts have been made to explore the dynamic behaviors and potential applications of MC circuits in a wide range of areas such as non-volatile memories, low-power computation, biological systems, oscillators, and filters.[6–11]

Currently, since MC is not commercially available, many emulating methods have been proposed to investigate their equivalent dynamic behaviors. A mutator capable of achieving bidirectional transformations between MR and MC has been proposed in Ref. [12] by making use of only three off-the-shelf active devices. A concise but effective interface circuit was designed in Ref. [13] for transforming MR into a memcapacitive system. Based on the constitutive relation, behavioral models of MC system were also established by making use of PSPICE simulation in Ref. [14]. The emulator of a practical floating MC without grounded restriction was designed in Ref. [15], which can be practically applied to electronic circuits. The method of emulating floating MCs with piecewise-linear constitutive relations was proposed based on multiple-state floating capacitor and implemented by using the switched-capacitor.[16] Dynamic behaviors of multi MCs in different connections were discussed by virtue of the MC emulators. The theoretical investigations of two MCs connected in series and parallel are presented in Ref. [17] by considering the mismatch effect of mobility factor and polarities. An efficient method to build the MC emulator in various configurations was firstly proposed in Ref. [18] by utilizing expandable MR emulator, and the dynamic behaviors of MC emulators in serial, parallel and hybrid as well as Wye (Y) and Delta (Δ) connections with multiple input sources were then discussed.

The MC-based oscillation circuitry is an attractive topic recently emerging in nonlinear electronic systems. The boundary dynamic behaviors of the charge-controlled MC for Joglekar's window function that describes the nonlinearities of the MC boundaries have been discussed in Ref. [19], of which the dynamic behaviors and necessary oscillation conditions of two configurations of the MC-based relaxation oscillator (RO) were theoretically analyzed in detail. A resistive-less RO where the RC circuit branch is replaced by two MRs or an

*Project supported by the Fundamental Research Funds for China Central Universities (Grant No. 2015XKMS028).

†Corresponding author. E-mail: dongsiee@163.com

© 2017 Chinese Physical Society and IOP Publishing Ltd

MR and a capacitor to emulate charging and discharging of RC circuit was presented in Ref. [20], of which the necessary conditions for oscillation and the generalized closed-form expression of the oscillation frequency were also derived. A Hewlett-Packard MR model and a charge-controlled MR model were presented in Ref. [21], and a new chaotic oscillator circuit based on the two models for exploring the characteristics of MRs and MCs in nonlinear circuits were designed. It has been proved that nonlinear MCs can be utilized to construct various oscillators.[22,23]

Recently, coupling has been defined as the third relation beyond series and parallel connections of memristive circuits in Ref. [24], where the mechanical coupling of two MCs was taken into account for illustrative example. The existence of coupling connection of two or multi MCs could provide us with more opportunities for developing new electronic devices with unique functions. Two relaxation oscillators interfaced by the coupling relation of two coupled MCs were presented in Ref. [25], of which the output oscillation frequency and duty cycle of one relaxation oscillator could be controlled by the other relaxation oscillator via the coupling strength. However, the dynamic behaviors of the coupled MCs were not well discussed in Ref. [25]. Dynamic behaviors of the coupled MCs deserve to be paid essential attention due to their uniqueness and complexity.

In this paper, by considering the coupling connections, the dynamic behaviors of two flux controlled MCs operated in serial and parallel connection with regards to identical or opposite polarities are systematically and mathematically discussed for the first time based on the constitutive relation. The equivalent memcapacitance (MCA) of two coupled MCs with different connection scenarios is theoretically calculated. Then, in order to further verify the theoretical analysis and the potential application of this coupled MCs with unique characteristics, this two coupled MCs in different serial and parallel connections are used for structuring RO by replacing the normal capacitor. In virtue of the coupling action, the output oscillation period and duty cycle are expected to be flexibly controlled. Finally, the multiple connection coupled MCs and coupled MC-based ROs are experimentally implemented to validate the correction of the theoretical calculation with numerical simulation.

2. Coupled MCs

As defined in Ref. [2], MCs can be classified as ρ-controlled MC and φ-controlled MC, where ρ and φ are the time integrals of charge $q(t)$ and voltage $v(t)$, respectively. The constitutive relation between charge and voltage of a flux controlled MC can be described as

$$q(t) = C_{\mathrm{m}}(\varphi)v(t), \tag{1}$$

where C_{m} denotes the MCA.

The existence of coupling actions of two or multi inductors and capacitors in electric circuits via magnetic or electric fields has been well known. It can be deduced that coupling action could be found between two MCs, which can physically influence or be influenced by the state-variable(s) of the other MC. Since charge and voltage are two intrinsic state variables relating to MCA, two MCs with coupling can be considered as coupled either by charge or by voltage as shown in Fig. 1. Based on Eq. (1), the flux controlled MC system with coupling can be described by the following set of equations,

$$q_1(t) = C_{\mathrm{m1}}(\varphi_1, \varphi_2)v_1(t), \tag{2a}$$

$$q_2(t) = C_{\mathrm{m2}}(\varphi_2, \varphi_1)v_2(t), \tag{2b}$$

$$\frac{\mathrm{d}\varphi_1}{\mathrm{d}t} = v_1(t), \quad \frac{\mathrm{d}\varphi_2}{\mathrm{d}t} = v_2(t). \tag{2c}$$

Many MC emulators with different constitutive relations have been proposed to exhibit the dynamic behaviors of flux controlled MC circuits. In this section, a linear flux-controlled MC is demonstratively adopted for discussion due to its simplicity and can be expressed as

$$C_{\mathrm{m}}(\varphi) = \alpha\varphi + \beta, \tag{3}$$

where α determines the variation rate of MCA and β is regarded as the initial MCA value.

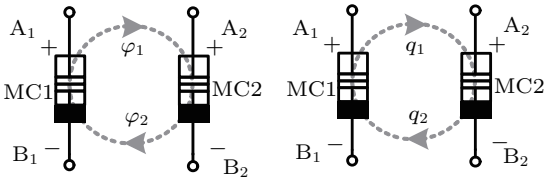


Fig. 1. Dual coupled MCs.

In accordance with Eqs. (2) and (3), the individual MCA of two flux-controlled coupled MCs can be described as

$$C_{\mathrm{m1}}(\varphi_1, \varphi_2) = \alpha_1\varphi_1 + \beta_1 + \kappa_2\varphi_2, \tag{4a}$$

$$C_{\mathrm{m2}}(\varphi_2, \varphi_1) = \alpha_2\varphi_2 + \beta_2 + \kappa_1\varphi_1. \tag{4b}$$

In accordance with Eq. (4), the coupling strength between these two MCs can be explained by the two coupling coefficients κ_1 and κ_2. Also, the coupling strength of these two MCs can easily become strong or weak by adjusting the coefficients κ_1 and κ_2. The coupling action between these two MCs as connected in serial or parallel connections can result in new attractive behaviors.

By making use of the linear flux-controlled MCA, the theoretical calculations and experimental implementations of these two coupled MCs can be greatly simplified. Also, the coupling influence from one MC on the dynamic behaviors of the other MC could be analytically illustrated.

3. Coupled MCs in serial connection

Two serial connection scenarios of dual coupled MCs are shown in this section with regards to identical and opposite polarities, respectively.

3.1. Serial MC circuit with identical polarities

By connecting terminal B_1 to A_2, two coupled MCs can be structured as a serial circuit with identical polarities as shown in Fig. 2. By using Kirchhoff's Voltage Law (KVL), the voltage and current across A_1 and B_2 can be written as

$$v_{12} = v_1 + v_2, \tag{5a}$$
$$i = i_1 = i_2. \tag{5b}$$

By integrating both sides of Eqs. (5a) and (5b), we have

$$\varphi_{12} = \varphi_1 + \varphi_2, \tag{6a}$$
$$q_{12} = q_1 = q_2. \tag{6b}$$

Based on Eqs. (1), (4), (5), and (6), the following set of differential equations for describing this serial circuit can be obtained:

$$\frac{\mathrm{d}\varphi_1}{\mathrm{d}t} = \frac{v_{12}(\alpha_2\varphi_2 + \beta_2 + \kappa_1\varphi_1)}{(\alpha_1+\kappa_1)\varphi_1 + (\alpha_2+\kappa_2)\varphi_2 + \beta_1 + \beta_2}, \tag{7a}$$
$$\frac{\mathrm{d}\varphi_2}{\mathrm{d}t} = \frac{v_{12}(\alpha_1\varphi_1 + \beta_1 + \kappa_2\varphi_2)}{(\alpha_1+\kappa_1)\varphi_1 + (\alpha_2+\kappa_2)\varphi_2 + \beta_1 + \beta_2}. \tag{7b}$$

Since equation (7) is too complex to be resolved by using analytical methods, numerical methods are generally used to calculate φ_1 and φ_2, as well as the MCA of each MC.

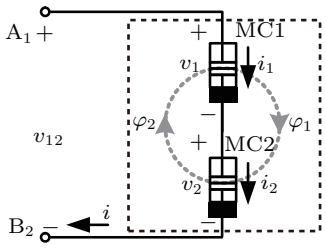


Fig. 2. Coupled MCs serially connected with identical polarities.

For the special case of $\alpha_1 = \alpha_2 = \kappa_1 = \kappa_2 = \alpha$, which can be precisely achieved by physical fabrication, equation (7) can be simplified into

$$\frac{\mathrm{d}\varphi_1}{\mathrm{d}t} = \frac{\alpha\varphi_{12} + \beta_2}{2\alpha\varphi_{12} + \beta_1 + \beta_2} v_{12}, \tag{8a}$$
$$\frac{\mathrm{d}\varphi_2}{\mathrm{d}t} = \frac{\alpha\varphi_{12} + \beta_1}{2\alpha\varphi_{12} + \beta_1 + \beta_2} v_{12}. \tag{8b}$$

Assuming that the initial values of φ_1 and φ_2 are both zero, the analytical expressions for φ_1 and φ_2 can be obtained as follows:

$$\varphi_1 = \frac{1}{2}\varphi_{12} + \frac{1}{4\alpha}(\beta_2 - \beta_1)\ln(2\alpha\varphi_{12} + \beta_1 + \beta_2), \tag{9a}$$
$$\varphi_2 = \frac{1}{2}\varphi_{12} + \frac{1}{4\alpha}(\beta_1 - \beta_2)\ln(2\alpha\varphi_{12} + \beta_1 + \beta_2). \tag{9b}$$

Hence, the MCA of individual MC can be obtained by substituting Eq. (9) into Eq. (4). For further simplification we assume that the initial MCA values β_1 and β_2 are both equal to β, equation (9) can be further simplified into

$$\varphi_1 = \varphi_2 = \frac{1}{2}\varphi_{12}, \quad v_1 = v_2 = \frac{1}{2}v_{12}. \tag{10}$$

According to Eqs. (4) and (10), the MCA of each MC can be expressed as

$$C_{\mathrm{m1}} = C_{\mathrm{m2}} = \alpha\varphi_{12} + \beta. \tag{11}$$

Based on the preceding analysis, it can be observed that two coupled MCs serially connected with identical polarities can be operated also as the MC but with new MCA value

$$C_{\mathrm{m12}} = \frac{C_{\mathrm{m1}}C_{\mathrm{m2}}}{C_{\mathrm{m1}} + C_{\mathrm{m2}}} = \frac{\alpha\varphi_{12}(t) + \beta}{2}. \tag{12}$$

For the special case of $\alpha_1 = \kappa_2 = 0$, these two MCs are in fact operated in serial connection without coupling effect. Besides, as $\alpha_1 = \alpha_2 = \alpha$ and $\beta_1 = \beta_2 = \beta$, the values of C_{m1} and C_{m2} can be expressed as

$$C_{\mathrm{m1}} = C_{\mathrm{m2}} = \frac{1}{2}\alpha\varphi_{12} + \beta. \tag{13}$$

3.2. Serial MC circuit with opposite polarities

By connecting B_1 to B_2, the diagram of two coupled MCs in serial connection with opposite polarities is shown in Fig. 3, where the excitation voltage v_{12} is applied to terminals A_1 and A_2, while terminal T is floating. The voltage, flux, current and charge of this circuit can be expressed by

$$v_{12} = v_1 + v_2, \quad \varphi_{12} = \varphi_1 + \varphi_2, \tag{14a}$$
$$i = i_1 = i_2, \quad q_{12} = C_{\mathrm{m1}}v_1 = C_{\mathrm{m2}}v_2. \tag{14b}$$

Therefore, the following set of differential equations can be obtained:

$$\frac{\mathrm{d}\varphi_1}{\mathrm{d}t} = \frac{v_{12}(-\alpha_2\varphi_2 + \beta_2 + \kappa_1\varphi_1)}{(\alpha_1+\kappa_1)\varphi_1 - (\alpha_2+\kappa_2)\varphi_2 + \beta_1 + \beta_2}, \tag{15a}$$
$$\frac{\mathrm{d}\varphi_2}{\mathrm{d}t} = \frac{v_{12}(\alpha_1\varphi_1 + \beta_1 - \kappa_2\varphi_2)}{(\alpha_1+\kappa_1)\varphi_1 - (\alpha_2+\kappa_2)\varphi_2 + \beta_1 + \beta_2}. \tag{15b}$$

Like Eq. (7), neither of the analytical solutions for φ_1 and φ_2 can be obtained from equation (15). By taking the special case of $\alpha_1 = \alpha_2 = \kappa_1 = \kappa_2 = \alpha$ into consideration, equation (15) can be simplified into

$$\varphi_1 = \frac{2\alpha\varphi_{12} + \sqrt{(\beta_1+\beta_2)^2 + 4\alpha(\beta_2-\beta_1)\varphi_{12}} - \beta_1 - \beta_2}{4\alpha}, \tag{16a}$$
$$\varphi_2 = \frac{2\alpha\varphi_{12} - \sqrt{(\beta_1+\beta_2)^2 + 4\alpha(\beta_2-\beta_1)\varphi_{12}} + \beta_1 + \beta_2}{4\alpha}. \tag{16b}$$

Subsequently, C_{m1} and C_{m2} can be obtained by substituting Eq. (16) into Eq. (4), and the equivalent MCA can be expressed as $C_{\mathrm{m1}}C_{\mathrm{m2}}/(C_{\mathrm{m1}} + C_{\mathrm{m2}})$. For the case of $\kappa_1 = \kappa_2 = 0$, these two coupled MCs in serial connection with opposite polarities are in fact operated without coupling effects. Furthermore, as $\alpha_1 = \alpha_2 = \alpha$ and $\beta_1 = \beta_2 = \beta$, C_{m1} and C_{m2} can be calculated from

$$C_{\mathrm{m1}} = \frac{\alpha\varphi_{12} + \sqrt{4\beta^2 - \alpha^2\varphi_{12}^2}}{2}, \tag{17a}$$

$$C_{\mathrm{m2}} = \frac{-\alpha\varphi_{12} + \sqrt{4\beta^2 - \alpha^2\varphi_{12}^2}}{2}. \tag{17b}$$

For further analyzing the dynamic behavior of this coupled MC circuit, a normal capacitor is serially connected with this coupled MC circuit as shown in Fig. 3, where v_{12} represents the voltage across terminals T and A_2 instead of A_1 and A_2. The voltage v_{12}, flux φ_{12}, current i as well as charge q can be represented by

$$v_{12} = v_{\mathrm{C}} + v_1 + v_2, \quad \varphi_{12} = \varphi_{\mathrm{C}} + \varphi_1 + \varphi_2, \tag{18a}$$

$$i = i_{\mathrm{C}} = i_1 = i_2, \quad q = q_{\mathrm{C}} = q_1 = q_2. \tag{18b}$$

From Eqs. (1), (4), and (18), we can derive the following equations:

$$\frac{\mathrm{d}\varphi_1}{\mathrm{d}t} = v_{12}C_s(-\alpha_2\varphi_2 + \beta_2 + \kappa_1\varphi_1)F(\varphi_1, \varphi_2), \tag{19a}$$

$$\frac{\mathrm{d}\varphi_2}{\mathrm{d}t} = v_{12}C_s(\alpha_1\varphi_1 + \beta_1 - \kappa_2\varphi_2)F(\varphi_1, \varphi_2), \tag{19b}$$

where

$$\begin{aligned} &F(\varphi_1, \varphi_2) \\ &= [(\alpha_1\varphi_1 + \beta_1 - \kappa_2\varphi_2)(-\alpha_2\varphi_2 + \beta_2 + \kappa_1\varphi_1) \\ &\quad + C_s(\alpha_1\varphi_1 + \kappa_1\varphi_1 - \alpha_2\varphi_2 - \kappa_2\varphi_2 + \beta_1 + \beta_2)]^{-1}. \end{aligned} \tag{20}$$

From Eq. (19), it can be clearly disclosed that even a linear capacitor connected with this coupled MC circuit can result in high complexities in resolving flux and MCA. For the special case of $\alpha_1 = \alpha_2 = \alpha$, $\kappa_1 = \kappa_2 = \kappa$, and $\beta_1 = \beta_2 = \beta$, we have

$$\varphi_1 = \varphi_2 = \frac{\varphi_{12}C_s}{\beta + 2C_s}, \tag{21a}$$

$$C_{\mathrm{m1}} = C_{\mathrm{m2}} = \beta, \tag{21b}$$

$$C_{\mathrm{m}} = \frac{\beta}{2}, C_{\mathrm{m12}} = \frac{\beta C_s}{\beta + 2C_s}, \tag{21c}$$

where C_{m} is the MCA of two serially connected MCs. In this simplified case, the coupled MC circuit connected in series with opposite polarities evidently behaves as a regular capacitor with a capacitance value of $\beta/2$.

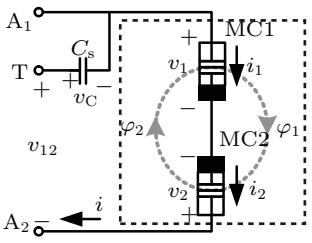


Fig. 3. Coupled MCs serially connected with opposite polarities.

4. Coupled MCs in parallel connection

The dual coupled MCs in parallel connection are studied in this section in terms of identical and opposite polarities.

4.1. Parallel MC circuit with identical polarity

The memcapacitive circuit of two coupled MCs in parallel connection with identical polarities is shown in Fig. 4, of which the current going through terminals A_1 and B_2, the charge, voltage and flux can be expressed by

$$i = i_1 + i_2, \quad q_{12} = q_1 + q_2. \tag{22a}$$

$$v_{12} = v_1 = v_2, \quad \varphi_{12} = \varphi_1 = \varphi_2. \tag{22b}$$

Hence, we have

$$\begin{aligned} q_{12} &= v_1(\alpha_1\varphi_1 + \beta_1 + \kappa_2\varphi_2) + v_2(\alpha_2\varphi_2 + \beta_2 + \kappa_1\varphi_1) \\ &= v_{12}(\alpha_1\varphi_1 + \kappa_1\varphi_1 + \alpha_2\varphi_2 + \kappa_2\varphi_2 + \beta_1 + \beta_2) \\ &= v_{12}[(\alpha_1 + \kappa_1 + \alpha_2 + \kappa_2)\varphi_{12} + \beta_1 + \beta_2]. \end{aligned} \tag{23}$$

By combining Eqs. (1) and (23), the total MCA of the dual coupled MCs in parallel connection can be calculated from

$$C_{\mathrm{m12}} = \frac{q_{12}}{v_{12}} = (\alpha_1 + \alpha_2 + \kappa_1 + \kappa_2)\varphi_{12} + \beta_1 + \beta_2. \tag{24}$$

Hence, it can be deduced from Eq. (24) that the flux coupled MCs in parallel connection can behave as a new flux-controlled MC, and the equivalent MCA value is equal to the sum of two individual MCAs.

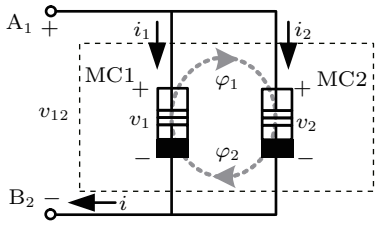


Fig. 4. Coupled MCs connected in parallel with the same polarities.

4.2. Parallel MC circuit with opposite polarity

The diagram of two coupled MCs connected in parallel with opposite polarities is shown in Fig. 5, the current, charge, voltage and flux can be shown by

$$i = i_1 + i_2, \quad q_{12} = q_1 + q_2, \tag{25a}$$

$$v_{12} = v_1 = v_2, \quad \varphi_{12} = \varphi_1 = \varphi_2. \tag{25b}$$

Based on Eq. (1) and (25a), it can be derived that

$$\begin{aligned} q_{12} &= v_1(\alpha_1\varphi_1 + \beta_1 - \kappa_2\varphi_2) + v_2(-\alpha_2\varphi_2 + \beta_2 + \kappa_1\varphi_1) \\ &= v_{12}(\alpha_1\varphi_1 + \kappa_1\varphi_1 - \alpha_2\varphi_2 - \kappa_2\varphi_2 + \beta_1 + \beta_2) \\ &= v_{12}[(\alpha_1 + \kappa_1 - \alpha_2 - \kappa_2)\varphi_{12} + \beta_1 + \beta_2]. \end{aligned} \tag{26}$$

By combining Eq. (1) with Eq. (26), the total MCA of the coupled MCs in parallel connection can be calculated by

$$C_{\mathrm{m12}}(\varphi_{12}) = \frac{q_{12}}{v_{12}} = (\alpha_1 - \alpha_2 + \kappa_1 - \kappa_2)\varphi_{12} + \beta_1 + \beta_2. \tag{27}$$

Equation (27) reveals that the variation of MCA in terms of flux φ_{12} is dependent on the difference between $\alpha_1 + \kappa_1$ and $\alpha_2 + \kappa_2$. For the case of $\alpha_1 + \kappa_1 > \alpha_2 + \kappa_2$, the MCA

is in direct proportion to the excitation flux φ_{12}, and higher flux will result in greater MCA. Likewise, for the case of $\alpha_1+\kappa_1<\alpha_2+\kappa_2$, the MCA is inversely proportional to flux φ_{12}, and the MCA decreases with the increase of flux. For the special case of $\alpha_1+\kappa_1=\alpha_2+\kappa_2$, this coupled MC is operated as a linear capacitor with the capacitance of $\beta_1+\beta_2$ independent of flux φ_{12}.

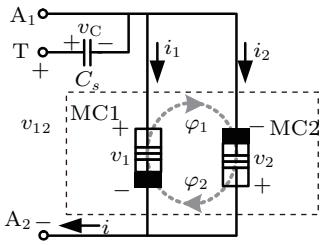


Fig. 5. Coupled MCs connected in parallel with opposite polarities.

Based on Eqs. (24) and (27), it can be observed that for the uncoupled case of $\kappa_1=\kappa_2=0$, the parallel connected MCs are also operated as a new MC but the MCA variation differs from the parallel MCs with coupling effect.

In order to further evaluate the coupled-MC-based parallel circuit, a common capacitor is serially connected with this dual coupled MC as shown in Fig. 5. The excitation voltage v_{12} is now imposed on terminals T and A_2 instead of A_1 and A_2. According to KVL and KCL, the following set of equations can be deduced:

$$i=i_1+i_2,\quad q=q_1+q_2, \tag{28a}$$

$$v_{12}=v_{\rm C}+v_1,\quad \varphi_{12}=\varphi_{\rm C}+\varphi_1, \tag{28b}$$

$$v_1=v_2,\quad \varphi_1=\varphi_2, \tag{28c}$$

where $v_{\rm C}$ is the voltage across capacitor C_s. From Eq. (27) it can be deduced that the MCA of the two coupled MCs is

$$C_{\rm m}(\varphi_1)=(\alpha_1+\kappa_1-\alpha_2-\kappa_2)\varphi_1+\beta_1+\beta_2. \tag{29}$$

By combining Eqs. (26) and (28a), we have

$$q=C_{\rm m1}v_1+C_{\rm m2}v_2=(C_{\rm m1}+C_{\rm m2})v_1. \tag{30}$$

Based on Eqs. (28a) and (30), the following equation holds:

$$v_{12}=v_{\rm C}+v_1=\frac{(C_{\rm m1}+C_{\rm m2})v_1}{C_s}+v_1. \tag{31}$$

By referring to Eq. (4) and integrating both sides of Eq. (31), the following equations can be obtained:

$$\varphi_1=\varphi_2=-\frac{\beta_1+\beta_2+C_s}{\alpha_1+\kappa_1-\alpha_2-\kappa_2}+\frac{\sqrt{(\beta_1+\beta_2+C_s)^2+2C_s(\alpha_1+\kappa_1-\alpha_2-\kappa_2)\varphi_{12}}}{\alpha_1+\kappa_1-\alpha_2-\kappa_2}, \tag{32a}$$

$$v_1=v_2=\frac{C_s v_{12}}{\sqrt{(\beta_1+\beta_2+C_s)^2+2C_s(\alpha_1+\kappa_1-\alpha_2-\kappa_2)\varphi_{12}}}. \tag{32b}$$

Therefore, the equivalent MCA across terminals T and A_2 can be analytically expressed as

$$C_{\rm m}=1-\frac{C_s^2}{\sqrt{(\beta_1+\beta_2+C_s)^2+2C_s(\alpha_1+\kappa_1-\alpha_2-\kappa_2)\varphi_{12}}}. \tag{33}$$

It can be concluded from Eq. (33) that when the coupled MCs are serially connected with a capacitor, the MCA value of the circuit is only dependent on the flux φ_{12} (or voltage v_{12}) across the terminals T and A_2.

It is worth noting that the coupling coefficients κ_1 and κ_2 can be positive or negative. Positive coefficient indicates coupling reinforcement while the negative one manifests counteraction of coupling effects.

5. Coupled-MCs-based relaxation oscillator

In order to comprehensively investigate the dynamic behaviors of coupled-MCs-based circuits and their potential applications, the two coupled MCs in serial and parallel connections both with opposite polarities are adopted to structure the relaxation oscillator circuit for demonstrative analysis.

5.1. Coupled MCs in serial connection and their RO

The coupled MCs connected in series with opposite polarities are used to structure an RO as shown in Fig. 6. According to input and output performance of the operational amplifier U1, we have

$$i_{\rm m}=C_{\rm m12}\frac{{\rm d}v_{\rm A1A2}}{{\rm d}t},\quad i_{\rm m}=\frac{v_{\rm o}-v_{\rm A1A2}}{R_{\rm s1}}. \tag{34}$$

Based on Eqs. (4) and (34), the set of system equations for describing the RO can be expressed by

$$\begin{cases}\dfrac{{\rm d}v_{\rm A1A2}}{{\rm d}t}=\dfrac{v_{\rm o}-v_{\rm A1A2}}{C_{\rm m12}R_{\rm s1}},\\[2ex] \dfrac{{\rm d}\varphi_{\rm A1A2}}{{\rm d}t}=v_{\rm A1A2}.\end{cases} \tag{35}$$

By setting $\alpha_1=\alpha_2=\kappa_1=\kappa_2=\alpha$, the equivalent MCA can be expressed by

$$C_{\rm m12}=\frac{C_{\rm m1}C_{\rm m2}}{C_{\rm m1}+C_{\rm m2}}, \tag{36}$$

where

$$\begin{cases}C_{\rm m1}(\varphi_1,\varphi_2)=\alpha\varphi_1+\beta_1-\alpha\varphi_2,\\ C_{\rm m2}(\varphi_2,\varphi_1)=-\alpha\varphi_2+\beta_2+\alpha\varphi_1,\\ \varphi_1=\dfrac{2\alpha\varphi_{12}+\sqrt{(\beta_1+\beta_2)^2+4\alpha(\beta_2-\beta_1)\varphi_{\rm A1A2}}-\beta_1-\beta_2}{4\alpha},\\ \varphi_2=\dfrac{2\alpha\varphi_{12}-\sqrt{(\beta_1+\beta_2)^2+4\alpha(\beta_2-\beta_1)\varphi_{\rm A1A2}}+\beta_1+\beta_2}{4\alpha}.\end{cases} \tag{37}$$

Equation (35) displays the variation relationship between $v_{\rm o}$ and $v_{\rm A1A2}$. By adjusting the coupling coefficients κ_1 and κ_2,

the output voltage v_o can be purposely controlled. However, equation (35) is very complex and can hardly be solved analytically. Normally, the numerical method is suggestively employed to inspect the inherent dynamic behaviors and output performance of the RO. For the special case of $\alpha_1 = \alpha_2 = \alpha$, $\beta_1 = \beta_2 = \beta$, and $\kappa_1 = \kappa_2 = 0$, the calculations of C_{m1} and C_{m2} can be simplified and expressed by Eq. (17), then the set of system equations for describing the RO can be simplified into

$$\begin{cases} \dfrac{dv_{A1A2}}{dt} = \dfrac{2\sqrt{4\beta^2 - \alpha^2\varphi_{A1A2}^2}(v_o - v_{A1A2})}{(2\beta^2 - \alpha^2\varphi_{A1A2}^2)R_{s1}}, \\ \dfrac{d\varphi_{A1A2}}{dt} = v_{A1A2}. \end{cases} \tag{38}$$

In this case, with $\kappa_1 = \kappa_2 = 0$, the output voltage v_o is only controlled by v_{A1A2}.

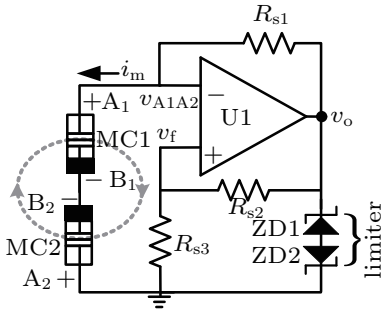


Fig. 6. Coupled MCs connected in series with opposite polarities and the RO.

5.2. Coupled MCs in parallel connection and its RO

The coupled MCs in parallel connection with opposite polarities are then used to build the RO, and the schematic diagram is shown in Fig. 7. Based on Eqs. (35), (36), and (27), the system functions of the coupled-MCs-based RO can be shown by

$$\begin{cases} \dfrac{dv_{A1B1}}{dt} = \dfrac{v_o - v_{A1B1}}{[(\alpha_1 - \alpha_2 + \kappa_1 - \kappa_2)\varphi_{A1B1} + \beta_1 + \beta_2]R_{s1}}, \\ \dfrac{d\varphi_{A1B1}}{dt} = v_{A1B1}, \end{cases} \tag{39}$$

where v_{A1B1} is equivalent to $-v_{A2B2}$ and v_o is controlled by v_{A1B1}. Meanwhile, by changing the values of κ_1 and κ_2 the output voltage of the RO can be controlled and operated inside the target range. For the uncoupled case of $\kappa_1 = \kappa_2 = 0$, the parallel MCs can also be operated as another MC with the MCA different from the parallel MCs with coupling effects. Also, the output voltage v_o is only determined by v_{A1B1} and we have

$$\begin{cases} \dfrac{dv_{A1B1}}{dt} = \dfrac{v_o - v_{A1B1}}{[(\alpha_1 - \alpha_2)\varphi_{A1B1} + \beta_1 + \beta_2]R_{s1}}, \\ \dfrac{d\varphi_{A1B1}}{dt} = v_{A1B1}. \end{cases} \tag{40}$$

Equation (40) possesses high nonlinearities and can hardly be analytically solved either. However, the voltage v_{A1B1} across MC1 can be calculated numerically.

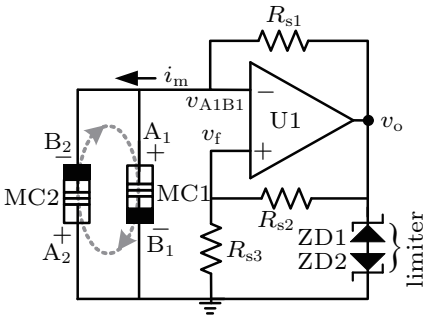


Fig. 7. Coupled MCs connected in parallel with opposite polarities and the RO.

6. Simulation analysis

In order to test the dynamic behaviors of dual coupled MC circuits and their application in RO circuit, simulation models are established based on the flux controlled constitutive relations.

6.1. Serial connections

The MCA of the serially connected MC circuit can be expressed as

$$C_{m12} = \frac{C_{m1}C_{m2}}{C_{m1} + C_{m2}}. \tag{41}$$

With regard to the case of serial connection with identical polarities, the simulation parameters are configured as $\alpha_1 = \alpha_2 = 4.914$ μF/Wb, $\beta_1 = \beta_2 = 0.5528$ μF, $\kappa_1 = 0.2\kappa_2$, and $\kappa_2 = \kappa_1$. A sinusoidal voltage of $v_{A1B2}(t) = 3\sin(20\pi t)$ V is adopted to excite this coupled-MC-based circuit. Based on Eq. (9), for consistence with theoretical analysis, the initial condition of $\varphi_1(0) = \varphi_2(0) = 0$ Wb is considered in the remaining simulation studies. Three curves of voltage versus charge corresponding to two individual MCs and the coupled MC in serial connection are shown in Fig. 8(a). It can be seen that the serially connected coupled MC circuit also possesses typical memcapacitive characteristics with pinched hysteresis loops (PHLs) behaving as an inclined "8". The voltage across MC1 with the amplitude of 1.028 V is clearly less than the voltage across MC2, which indicates that the MCAof C_{m1} is time variant and greater than C_{m2}.

Three curves of MCA varying with current are shown in Fig. 8(b), which demonstrates that the MCA of the dual coupled MCs in serial connection is less than the individual MCAs C_{m1} or C_{m2}. The MCAs increases with the increase of the current passing through them. The variations of intervals C_{m1}, C_{m2}, and C_{m12} are measured to be [0.634,1.013], [0.329,0.529], and [0.217,0.347] μF, respectively.

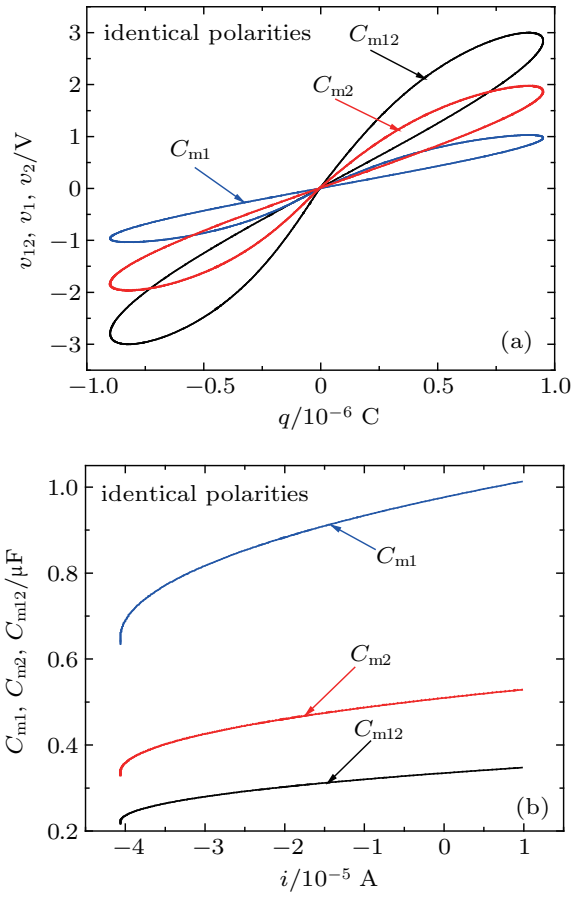


Fig. 8. (color online) Simulation results of serial connection. (a) PHLs; (b) Curves of MCA varying with current.

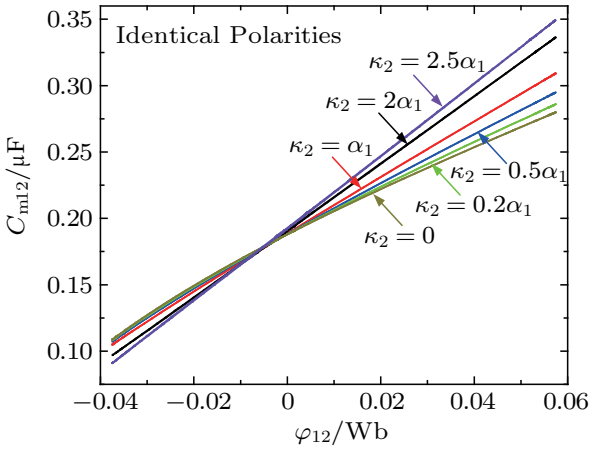


Fig. 9. (color online) Curves of MCA varying with flux under the conditions of different values of coupling coefficient κ_2.

For observing the influence of coupling coefficients on MCA C_{m12}, different values of coupling coefficient κ_2 are chosen. Curves of MCA varying with flux under the condition of different values of coupling coefficient κ_2 are shown in Fig. 9, from which we can see that the MCA C_{m12} can increase from the initial value 0.093 μF with the increase of flux under the condition of coefficients κ_2 varying from 0 to $2.5\alpha_1$. The curve slope of C_{m12} versus φ_{12} can also increases with the increase of coefficient κ_2.

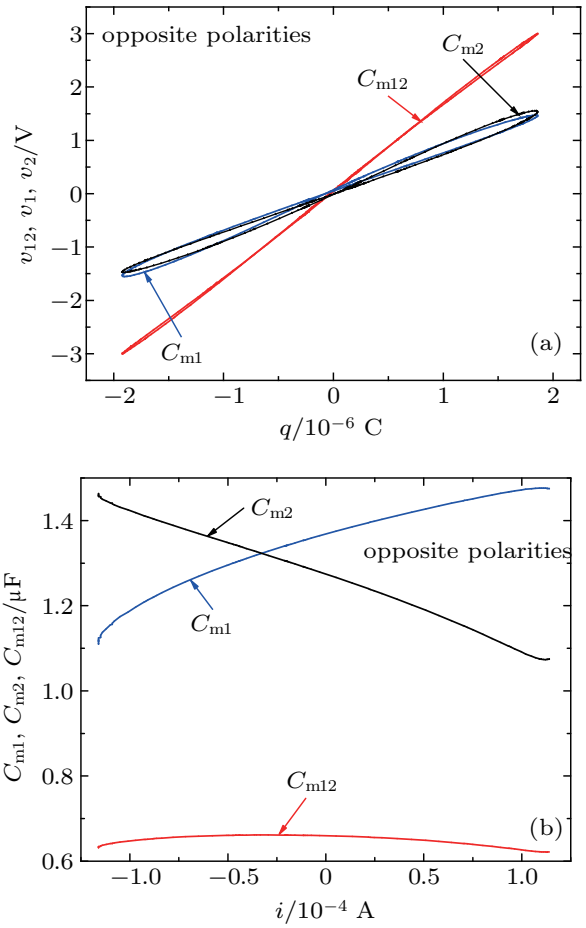


Fig. 10. (color online) Simulation results of serial connection. (a) PHLs; (b) Curves of MCA varying with current.

For the connection condition with opposite polarities, the simulation parameters are configured as $\alpha_1 = \alpha_2 = 0.1659$ μF/Wb, $\beta_1 = \beta_2 = 1.269$ μF, $\kappa_1 = 0.5\alpha_2$, and $\kappa_2 = 0.5\alpha_1$. A sinusoidal voltage of $v_{A1A2}(t) = 3\sin(20\pi t)$ V is used for exciting the coupled MC circuit. Three curves of voltage versus charge corresponding to two individual MCs and the coupled MC circuit are shown in Fig. 10(a). Like the case of identical polarities, the two serial MCs also behave together as a new MC with PHL passing through the origin. The MCAs of C_{m1}, C_{m2}, and C_{m12} in terms of current are shown in Fig. 10(b). Unlike the case of identical polarities, the C_{m1} can be nonlinearly increased by increasing the current, and the C_{m2} can nonlinearly decrease, while the MCA C_{m12} first increases and then decreases. For the maximal charge quantities, the values of C_{m1}, C_{m2}, and C_{m12} are 1.475, 1.075, and 0.622μF, respectively. Figure 11 shows the variation characteristics of MCA against flux, with κ_1 changing from $0.039\alpha_1$ to α_1. Obviously, the curve of C_{m12} versus φ_{12} first increases and then decreases when κ_1 is equivalent to $0.039\alpha_2$, $0.39\alpha_2$, and $0.5\alpha_2$, respectively, and then values of C_{m12} reach maximal values of 0.6224, 0.6209, and 0.6196 μF respectively when $\varphi_{12} = -0.0193$ Wb.

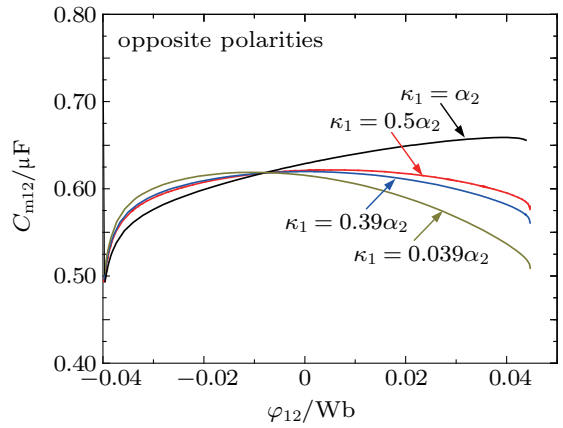


Fig. 11. (color online) Curves of MCA varying with flux under the condition of different values of coupling coefficient κ_1.

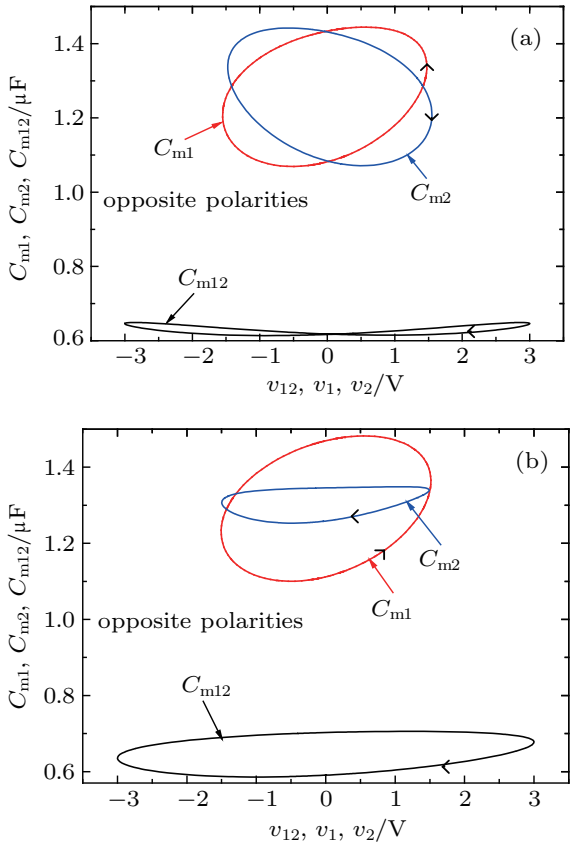


Fig. 12. (color online) Curves of MCA varying with terminal voltage. (a) $\kappa_1 = 0.5\alpha_2$ and $\kappa_2 = 0.5\alpha_1$; (b) $\kappa_1 = 0.5\alpha_2$ and $\kappa_2 = \alpha_1$.

According to the preceding analysis, the voltage across each MC also periodically evolves but no longer sinusoidally due to nonlinear variation of MCA. The curves of MCAs C_{m1}, C_{m2}, and C_{m12} varying with terminal voltage v_1, v_2, and v_{12} are displayed in Fig. 12 for comparatively analyzing the influences from different coupling coefficients. The curve of C_{m1} versus v_1 evolves anticlockwise, which means that positive v_1 results in the increase of C_{m1} and negative v_1 leads to the decrease of C_{m1}. The curves of C_{m2} versus v_2 and C_{m12} versus v_{12} evolve clockwise, corresponding to the alternating voltages v_2 and v_{12}, respectively. In consideration of the symmetry, only the positive interval is needed for demonstration. When two MCs are positively coupled with $\kappa_1 = 0.5\alpha_2$ and $\kappa_2 = 0.5\alpha_1$, C_{m12} first increases and then decreases with the positive voltage increasing as shown in Fig. 12(a). However, C_{m12} is monotonically decreased and the variation range of C_{m12} can be comparatively widened by $\kappa_1 = 0.5\alpha_2$ and $\kappa_2 = \alpha_1$ as shown in Fig. 12(b).

A regular capacitor of 330 nF is serially connected with the coupled MC circuit for further discovering the dynamic behaviors and connectivity of this serial memcapacitive circuit. Curves of MCA C_m varying with φ_m for different values of coupling coefficient κ_1 but constant coupling coefficient κ_2 ($\kappa_2 = 0.5\alpha_1$) are shown in Fig. 13(a). It reveals that $\kappa_1 \geq 0.66\alpha_2 C_m$ can nonlinearly increase with the increase of flux φ_m, while $0.39\alpha_2 \leq \kappa_1 < 0.66\alpha_2$, C_m can first increase and then decrease with the increase of flux φ_m. Evidently, for $\kappa_1 \leq 0.39\alpha_2$, C_m can nonlinearly decrease with the increment of flux φ_m. The enlarged curve of $\kappa_1 = 0.5\alpha_2$ is shown in Fig. 13(b) for demonstration.

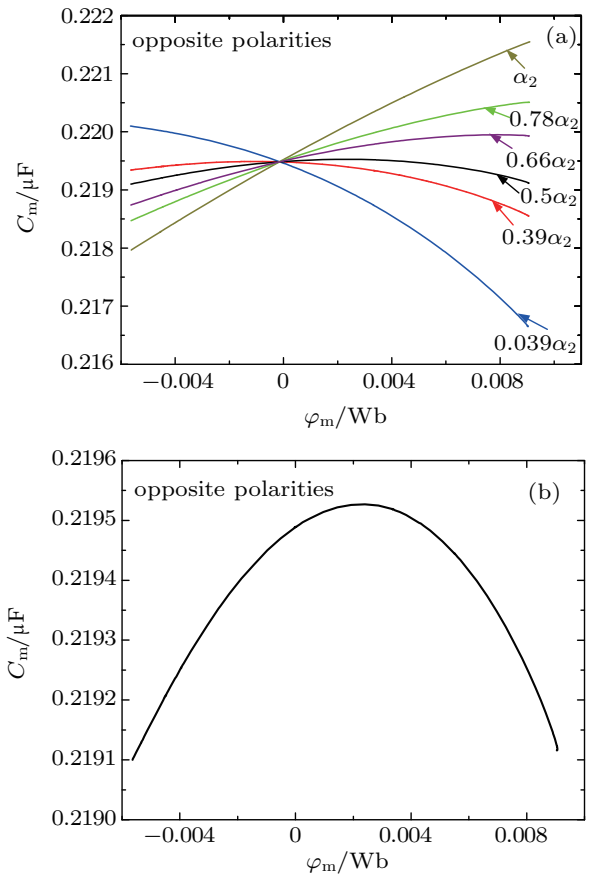


Fig. 13. (color online) Curves of MCA varying with flux. (a) κ_1 equivalent to $0.039\alpha_2$, $0.39\alpha_2$, $0.5\alpha_2$, $0.66\alpha_2$, $0.78\alpha_2$, and α_2; (b) Enlarged curve of $\kappa_1 = 0.5\alpha_2$.

6.2. Parallel connections

The MCA of the parallel connected coupled MC circuit can be expressed as

$$C_{m12} = C_{m1} + C_{m2}. \tag{42}$$

For the case of coupled MC in parallel connection with identical polarities, simulation parameters are employed as follows: $\alpha_1 = \alpha_2 = 16.59$ μF/Wb, $\beta_1 = \beta_2 = 1.269$ μF, $\kappa_1 = \alpha_2$, and $\kappa_2 = 0.5\alpha_1$. The curves of charge versus voltage corresponding to C_{m1}, C_{m2}, and C_{m12} behave as typical PHLs as shown in Fig. 14(a), which reveals that the two MCs in parallel connection can also be operated together as a new MC. The MCA of this memcapacitive circuit is shown in Fig. 14(b). The values of MCA C_{m12} vary with flux φ_{12} for different values of coupling strength κ_1. The magnitude of the MCA can be linearly enlarged by increasing the coupling strength κ_1 and κ_2, which is in good agreement with Eq. (24).

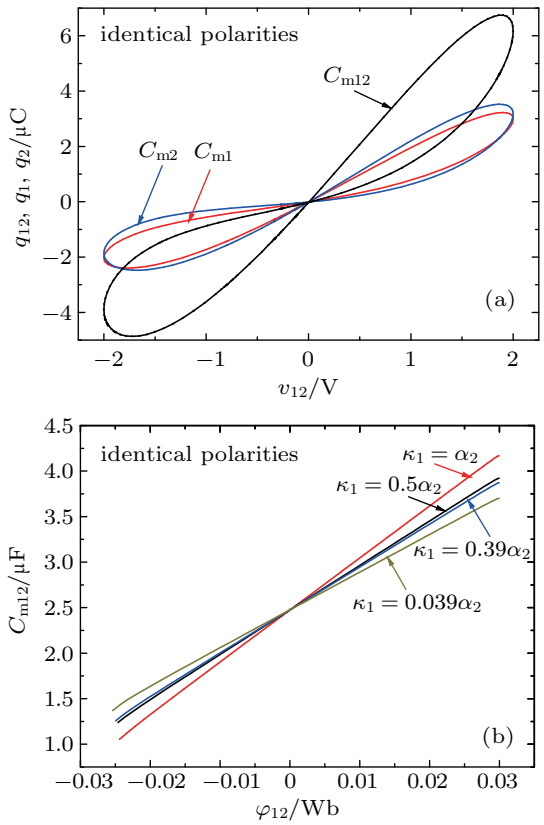


Fig. 14. (color online) Simulated curves of parallel connections. (a) PHLs; (b) MCA varying with flux for different values of κ_1.

The parameters configured for the two coupled MCs in parallel connection with opposite polarities are the same as those in the case of identical polarities. The variations of MCA C_{m12} with flux φ_{12} for different values of coupling coefficient κ_1, when κ_2 is equal to $0.5\alpha_1$, is depicted in Fig. 15. It can be observed that the MCA constantly remains at 2.558 μF for the special case of $\kappa_1 = \kappa_2 = 0.5\alpha_1$. For the case of $\kappa_1 < \kappa_2$, the MCA linearly decreases with increasing the flux while the MCA can linearly increase with the flux increasing as $\kappa_1 > \kappa_2$, which is in good agreement with Eq. (29).

The simulated curves of MCAs varying with charge for the case of $\kappa_1 = 0.39\alpha_2$ and $\kappa_2 = 0.5\alpha_1$ are shown in Fig. 16(a). Due to curve symmetry, only the interval of positive charge is needed for demonstration. Unlike C_{m2} and C_{m12}, C_{m1} can increase with the increase of positive charge. The maximal values of charge q_1 and C_{m1} are much less than q_{12} and C_{m12}, respectively. Curves of MCA for another coupling case of $\kappa_1 = 0.75\alpha_2$ and $\kappa_2 = 0.5\alpha_1$ are displayed in Fig. 17(a). In this case, both C_{m1} and C_{m2} can first increase and then decrease with increasing positive charge. Hence, C_{m12} can first increase and then decrease with the increase of positive charge. The waveforms of MCA and charge in time domain are correspondingly given in Figs. 16(b) and 17(b) for comparative illustration, respectively.

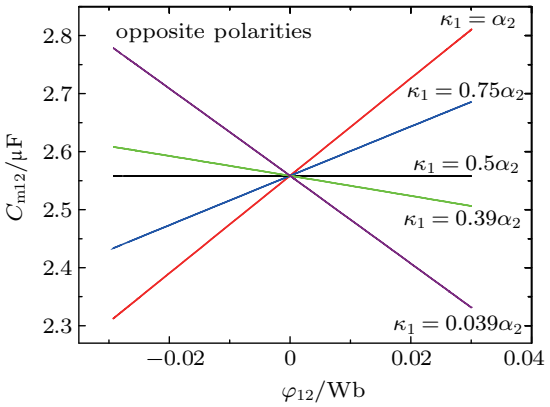


Fig. 15. (color online) Curves of MCA varying with flux for different values of coupling coefficient κ_2.

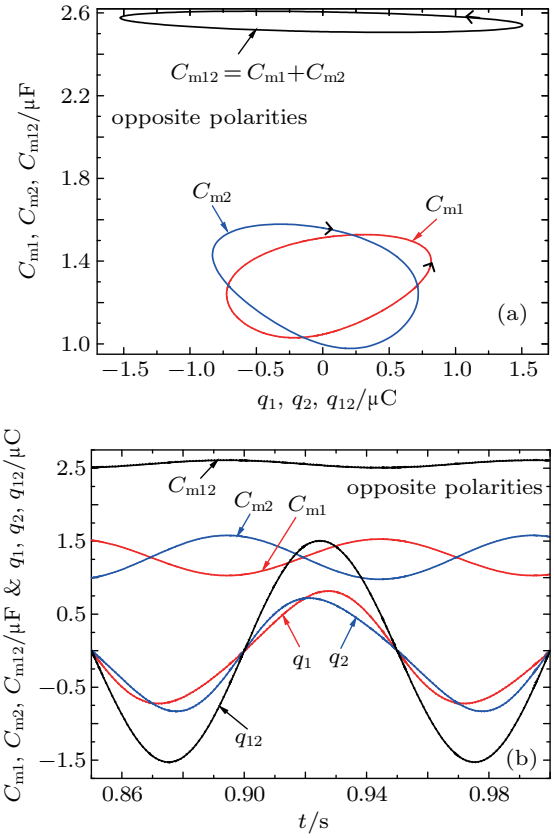


Fig. 16. (color online) Simulated curves of MCA and charge. (a) MCA varies with current for $\kappa_1 = 0.39\alpha_2$ and $\kappa_2 = 0.5\alpha_1$; (b) time-domain waveforms of MCA and charge.

A common capacitor of 330nF is serially connected to the coupled MC circuit with $\kappa_2 = 0.5\alpha_1$ for exploring the MCA

variation with flux as shown in Fig. 18. These results reveal that for the case of coupling strength κ_1 lower than κ_2, the MCA can decrease linearly with the increase of flux. While κ_1 is greater than κ_2, the MCA can linearly increase with the increase of flux. Note that for the case of $\kappa_1 = \kappa_2 = 0.5\alpha_1$, the equivalent MCA keeps unchanged and equal to the sum of β_1 and β_2.

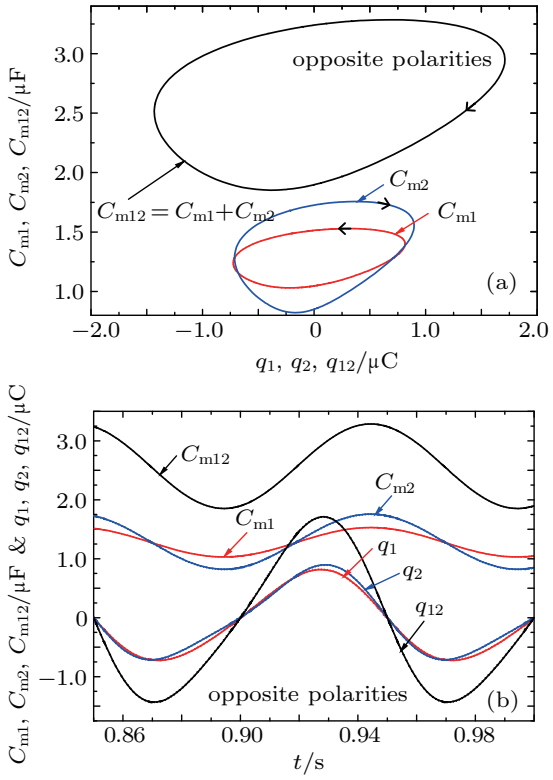


Fig. 17. (color online) Simulated curves MCA and charge. (a) MCA curves varying with current for $\kappa_1 = 0.75\alpha_2$ and $\kappa_2 = 0.5\alpha_1$; (b) time-domain waveform of MCA and charge.

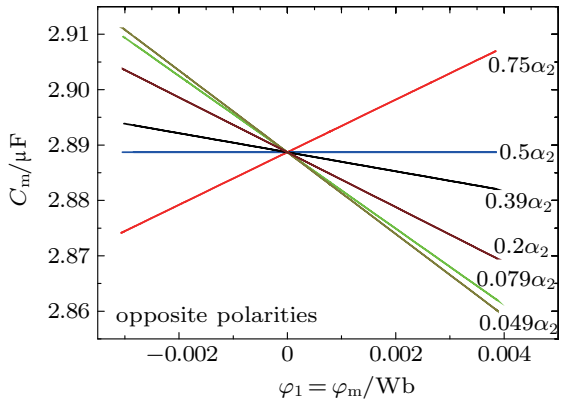


Fig. 18. (color online) Curves of MCA varying with flux for different values of coupling coefficient κ_1.

6.3. Coupled MCs based RO

The simulation results of coupled-MCs-based RO are demonstrated in this subsection for further discovering the possible practical application of the coupled MCs.

The RO circuit structured by the coupled MCs in serial connection with opposite polarities is first analyzed. The simulation parameters of the coupled MCs are configured as $\alpha_1 = \alpha_2 = 1.918$ μF/Wb, $\beta_1 = \beta_2 = 0.4315$ μF, $\kappa_1 = 0.087\alpha_2$, and $\kappa_2 = 0.071\alpha_1$. Three curves of voltage versus charge are displayed in Fig. 19(a), which indicates that the coupled MC circuit in serial connection also possesses the memcapacitive characteristics with pinched hysteresis loops (PHLs) behaving as an inclined "8". The maximal voltage across MC1 is 2.727 V, which is less than that of MC2. Besides, the minimal voltage across MC1 is −3.367 V, which is also less than that of MC2. The time-domain waveforms of voltage and charge are shown in Fig. 19(b) for comparative demonstration.

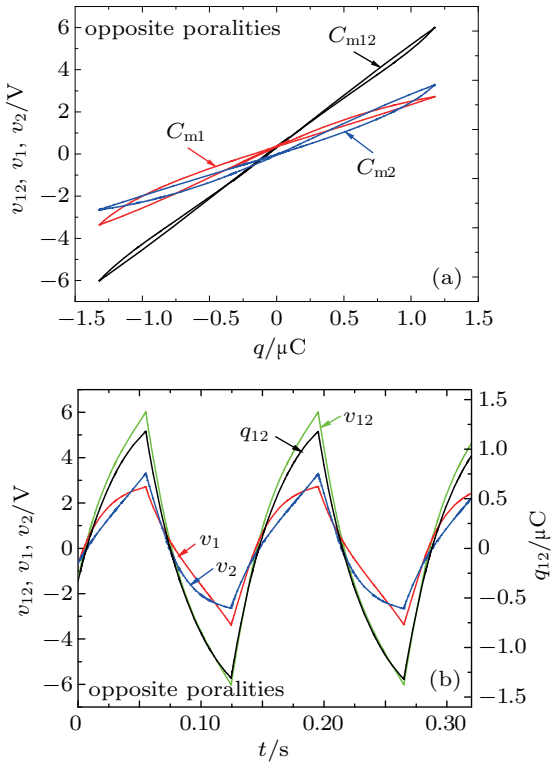


Fig. 19. (color online) Curves of voltage and charge. (a) PHLs; (b) time-domain waveforms of voltage and charge.

By configuring $R_{s1} = 200$ kΩ, $R_{s2} = 100$ kΩ, and $R_{s3} = 200$ kΩ, simulation figures are presented to display the output characteristics of the MC-based ROs as demonstratively shown in Fig. 20. The output oscillating period and duty cycle of the RO for $\kappa_1 = 3.9\alpha_2$ and $\kappa_2 = 0.071\alpha_1$ (Fig. 20(a)) are 235.55 ms and 62.4%, respectively. For the case of $\kappa_1 = 0.39\alpha_2$ and $\kappa_2 = 0.071\alpha_1$ as shown in Figs. 20(a) and 20(b), the output oscillating period and duty cycle of RO are 143.63 ms and 51.36%, respectively. Meanwhile, for the case of $\kappa_1 = 0.087\kappa_2$ and $\kappa_2 = 0.071\kappa_1$ (Fig. 20(b)), the output oscillating period and duty cycle of RO are measured to be 140.51 ms and 50.44%. Likewise, by changing the value of coupling coefficient κ_2, the oscillation period and duty cycle of the RO can also be regulated, which is in good agreement with the scenario in Fig. 20.

Then, the RO circuit established by the coupled MCs in parallel connection with opposite polarities is analyzed. The

simulation parameters of coupled-MCs-based RO are set to be as follows: $\kappa_1 = 3.9\alpha_2$, $\kappa_2 = 0.49\alpha_1$, $\alpha_1 = \alpha_2 = 1.918$ μF/Wb, $\beta_1 = \beta_2 = 0.4315$ μF, $R_{s1} = 200$ kΩ, $R_{s2} = 100$ kΩ, and $R_{s3} = 23$ kΩ. Three PHLs corresponding to C_{m1}, C_{m2}, and C_{m12} are shown in Fig. 21(a), which reveals that the coupled MCs in parallel connection have typical memcapacitive behaviors even when operated in the RO circuit. The measured maximal charge passing through MC1 in positive direction is 1.2686 μC, which is greater than that of MC2. The charge passing through MC1 in negative direction is −1.0658 μC, which is greater than that of MC2 as well. Hence, the intersection occurs between trajectories of C_{m1} and C_{m2} as shown in Fig. 21(b). These three curves shown in Fig. 21(b) are in good agreement with the theoretical calculations from Eqs. (25) and (27).

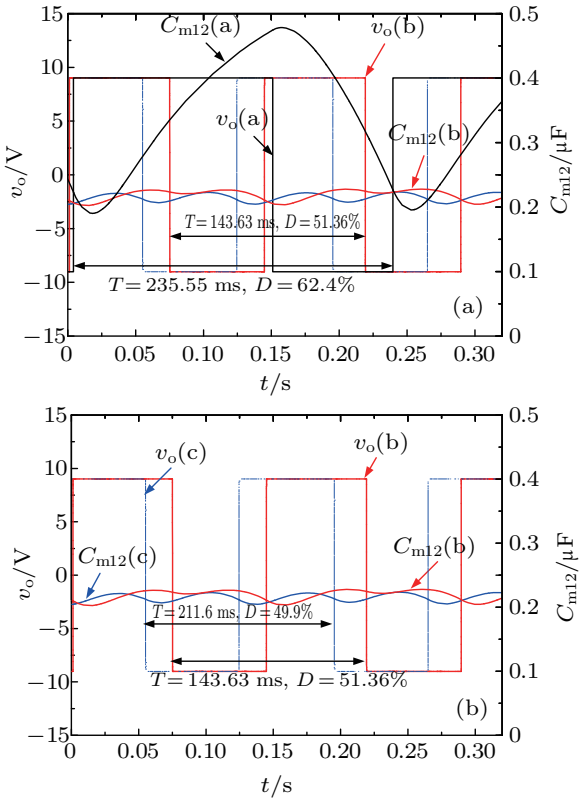


Fig. 20. (color online) Simulation results of serially connected coupled-MCs-based RO. (a) $\kappa_1 = 3.9\alpha_2$ and $\kappa_1 = 0.39\alpha_2$; (b) $\kappa_1 = 0.39\alpha_2$ and $\kappa_1 = 0.087\alpha_2$.

The waveforms of output voltage and MCA in time-domain are displayed in Fig. 22, which reveals the dynamic behaviors of the output oscillation voltage in terms of MCA. According to the simulation results exhibited by Figs. 20 and 22, we can see that high coupling coefficient κ_1 can actually lead to high periods and duty cycles. Also, as shown in Fig. 22, the output oscillation period and duty cycle of the RO for $\kappa_1 = 3.9\alpha_2$ and $\kappa_2 = 0.49\alpha_1$ (Fig. 22(a)) are measured to be 259.7 ms and 52.33%, respectively. For the operation case of $\kappa_1 = 0.078\alpha_2$ and $\kappa_2 = 0.49\alpha_1$ as shown in Figs. 22(a) and 22(b), the output oscillating period and duty cycle of the RO are 212.6 ms and 49.95%, respectively. Under the condition of $\kappa_1 = 0.039\alpha_2$ and $\kappa_2 = 0.49\alpha_1$ (Fig. 22(b)), the output oscillation period and duty cycle of the RO are 211.6 ms and 49.9%, respectively.

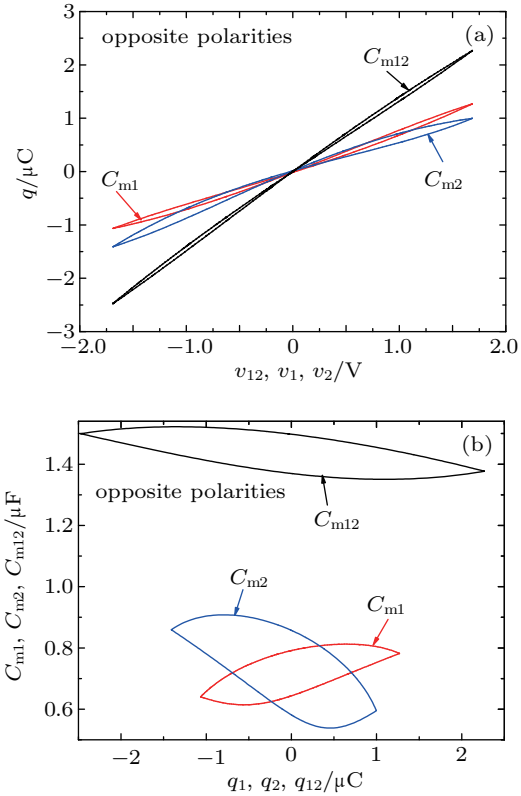


Fig. 21. (color online) Voltage, charge and MCA. (a) Charge varying with voltage; (b) MCA varying with charge.

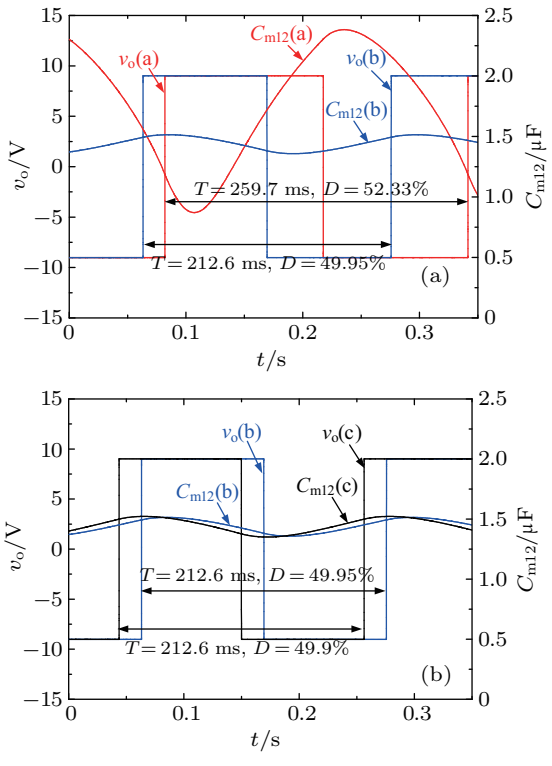


Fig. 22. (color online) Simulation results of coupled parallel connected MCs-based RO. (a) $\kappa_1 = 3.9\alpha_2$ and $\kappa_1 = 0.078\alpha_2$; (b) $\kappa_1 = 0.078\alpha_2$ and $\kappa_1 = 0.039\alpha_2$.

7. Experimental analysis

In order to practically observe the dynamic behaviors of the coupled MCs and the RO, an analog circuit which can emulate two flux-controlled coupled MCs is first designed and experimentally implemented. Then, these coupled MCs are configured with different connections for structuring the RO circuits. The experimental curves are sampled and analyzed to verify the correctness of theoretical and simulation results.

7.1. Coupled MC emulator

The proposed schematic of two coupled MC emulators is shown in Fig. 23. One op amp (TL084), one multiplier (AD633), and four current feedback op amps (CFOA) are necessarily required for building each of the two emulators, i.e., MC1 (inside the upper red dotted frame) and MC2 (inside the lower blue dotted frame). Without considering the coupling effects, by referring to the operational function of CFOA AD844, we have

$$v_{\mathrm{u}11} = \frac{R_{21}}{R_{11}} v_{\mathrm{A1B1}}, \tag{43a}$$

$$v_{\mathrm{u}31} = -\frac{1}{R_{11}C_1} \varphi_{\mathrm{A1B1}}, \tag{43b}$$

where φ_{A1B1} is the time integral of terminal voltage v_{A1B1}, v_{u11}, and v_{u31} are the output voltages of CFOAs U11 and U31, respectively. The coupling action is achieved by two adder circuits made by op amps U51 and U52.The output voltage of op amp U51 can be calculated from

$$v_{\mathrm{u}51} = \frac{R_{51}}{R_{31}R_{11}C_1} \varphi_{\mathrm{A1B1}} - \frac{R_{51}}{R_{41}} v_{\mathrm{s}1}. \tag{44}$$

Based on the datasheet of AD633, $v_{\mathrm{w}1}$ can be derived as

$$v_{\mathrm{w}1} = v_{\mathrm{u}51} \cdot v_{\mathrm{u}11} \frac{R_{61}+R_{71}}{10R_{61}}. \tag{45}$$

Due to the actions of U21 and U41, the current i_{MC1} going through terminals A_1 and B_1 is in fact determined by voltage $v_{\mathrm{w}1}$. Therefore, we have

$$i_{\mathrm{MC1}} = C_{1\mathrm{m}} \frac{\mathrm{d}v_{\mathrm{w}1}}{\mathrm{d}t}, \tag{46a}$$

$$q_{\mathrm{MC1}} = C_{1\mathrm{m}} v_{\mathrm{w}1}, \tag{46b}$$

where q_{MC1} is the time integral of i_{MC1}. By combining Eqs. (43a), (45) and (46b), we can deduce the following equation:

$$v_{\mathrm{u}51} = \frac{10R_{11}R_{61}}{R_{21}(R_{61}+R_{71})C_{1\mathrm{m}}} \cdot \frac{q_{\mathrm{MC1}}}{v_{\mathrm{A1B1}}}. \tag{47}$$

Hence, the MCA of MC1 can be derived by considering the coupling action,

$$C_{\mathrm{M1}}(\varphi_{\mathrm{A1B1}}) = \frac{q_{\mathrm{MC1}}}{v_{\mathrm{A1B1}}} = \alpha_1 \varphi_{\mathrm{A1B1}} + \beta_1, \tag{48}$$

where α_1 is corresponding to the variation rate of MCA, and parameters α_1 and β_1 can be expressed as

$$\alpha_1 = \frac{R_{21}R_{51}(R_{61}+R_{71})C_{1\mathrm{m}}}{10R_{11}^2R_{31}R_{61}C_1},$$

$$\beta_1 = -\frac{R_{21}R_{51}(R_{61}+R_{71})C_{1\mathrm{m}}}{10R_{11}R_{41}R_{61}} v_{\mathrm{s}1}. \tag{49}$$

Therefore, it can be deduced from Eq. (49) that the initial value of MCA can be adjusted by resistor R_{41} and DC voltage supply $v_{\mathrm{s}1}$.

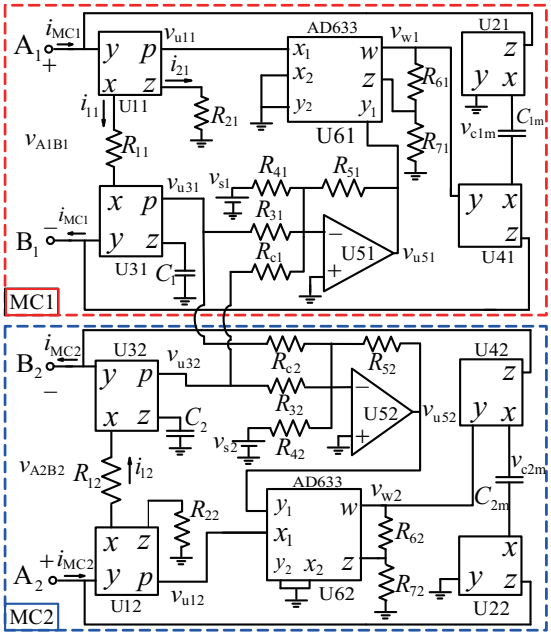


Fig. 23. (color online) Schematic diagram of two flux-controlled coupled MC emulators.

By taking the coupling strength into consideration, the coupling connection between MC1 and MC2 is achieved by two inverting adders (U51 and U52). According to Eqs. (44), (47), (48), and (49), the MCA of each MC can be expressed by

$$C_{\mathrm{M1}}(\varphi_{\mathrm{A1B1}}, \varphi_{\mathrm{A2B2}}) = \alpha_1 \varphi_{\mathrm{A1B1}} + \beta_1 + \kappa_2 \varphi_{\mathrm{A2B2}}, \tag{50a}$$

$$C_{\mathrm{M2}}(\varphi_{\mathrm{A2B2}}, \varphi_{\mathrm{A1B1}}) = \alpha_2 \varphi_{\mathrm{A2B2}} + \beta_2 + \kappa_1 \varphi_{\mathrm{A1B1}}, \tag{50b}$$

where the parameters α_2 and β_2 can be deduced by referring to Eqs. (48) and (49), and the coupling coefficients κ_1 and κ_2 are

$$\kappa_1 = \frac{R_{22}R_{52}(R_{62}+R_{72})C_{2\mathrm{m}}}{10R_{11}R_{12}R_{62}R_{\mathrm{c}2}C_1},$$

$$\kappa_2 = -\frac{R_{21}R_{51}(R_{61}+R_{71})C_{1\mathrm{m}}}{10R_{11}R_{12}R_{61}R_{\mathrm{c}1}C_2}. \tag{51}$$

Hence, the coupling strengths can be conveniently controlled by adjusting the values of coupling resistors $R_{\mathrm{c}1}$ and $R_{\mathrm{c}2}$ in the emulator as shown in Fig. 23.

In the experimental implementation, it has been confirmed that the possible variation range of the MCA is mainly dependent on the saturation output of the active chips. As

shown in Fig. 23, by taking MC1 for demonstration, U31 possesses the highest chance to be operated with saturation output, while the amplitude and period of the input voltage v_{A1B1} are both large. Assuming that the power supply voltages of the active chips are V_{OH} and V_{OL}, when positive saturation happens to U31, namely, $v_{u31} = V_{OH}$. According to Eq. (44), we have

$$v_{u51} = -R_{15}\left(\frac{V_{OH}}{R_{31}} + \frac{v_{s1}}{R_{14}} + \frac{v_{u32}}{R_{c1}}\right), \tag{52}$$

$$v_{w1} = v_{u51}v_{u11}\frac{R_{61}+R_{71}}{10R_{61}} = -\frac{R_{21}R_{51}(R_{61}+R_{71})}{10R_{11}R_{61}} \times \left(\frac{V_{OH}}{R_{31}} + \frac{v_{s1}}{R_{41}} + \frac{v_{u32}}{R_{c1}}\right), \tag{53}$$

$$q_{MC1} = C_{1m}v_{w1} = -v_{A1B1}\frac{R_{21}R_{51}(R_{61}+R_{71})C_{1m}}{10R_{11}R_{61}} \times \left(\frac{V_{OH}}{R_{31}} + \frac{v_{s1}}{R_{41}} + \frac{v_{u32}}{R_{c1}}\right). \tag{54}$$

Hence, the upper boundary of MCA variation range C_{M1max} can be calculated from

$$C_{M1max} = \frac{q_{MC1}}{v_{A1B1}} = -\frac{R_{21}R_{51}(R_{61}+R_{71})C_{1m}}{10R_{11}R_{61}} \times \left(\frac{V_{OH}}{R_{31}} + \frac{v_{s1}}{R_{41}} + \frac{v_{u32}}{R_{c1}}\right). \tag{55}$$

Likewise, when negative saturation to U31, $v_{u31} = V_{OL}$, the lower boundary of MCA variation range C_{M1min} can be obtained from

$$C_{M1min} = \frac{q_{MC1}}{v_{A1B1}} = -\frac{R_{21}R_{51}(R_{61}+R_{71})C_{1m}}{10R_{11}R_{61}} \times \left(\frac{V_{OL}}{R_{31}} + \frac{v_{s1}}{R_{41}} + \frac{v_{u32}}{R_{c1}}\right). \tag{56}$$

Similarly, saturation could happen to the adder circuit U51. For the case of $v_{u51} = V_{OH}$, according to Eq. (45), we have

$$v_{w1} = v_{u51}v_{u11}\frac{R_{61}+R_{71}}{10R_{61}} = v_{A1B1}V_{OH}\frac{R_{21}(R_{61}+R_{71})}{10R_{11}R_{61}}, \tag{57}$$

$$q_{MC1} = C_{1m}v_{w1} = v_{A1B1}V_{OH}\frac{R_{21}(R_{61}+R_{71})C_{1m}}{10R_{11}R_{61}}. \tag{58}$$

In this case, based on Eq. (58), the maximal value of MCA C_{M1max} can be expressed by

$$C_{M1max} = \frac{R_{21}(R_{61}+R_{71})C_{1m}V_{OH}}{10R_{11}R_{61}}. \tag{59}$$

Likewise, the minimal value of MCA C_{M1min} can be deduced by

$$C_{M1min} = \frac{R_{21}(R_{61}+R_{71})C_{1m}V_{OL}}{10R_{11}R_{61}}. \tag{60}$$

The saturation could also happen to the remaining active chips shown in Fig. 23. The value of MCA remains constant as the saturation takes place. Therefore, in the MC-based RO circuit, neither the output oscillation period nor duty cycle can be controlled by the coupling strength as the MCA reaches its maximal or minimal boundary. However, output saturations of the active chips could be avoided by properly adjusting the system parameters of the circuit, such as the values of the resistors.

7.2. Experimental analysis

The case of two coupled MC circuits serially combined with opposite polarities (B_1 directly connected to B_2) is taken for demonstration to verify the theoretical analysis. The experimental parameters are given as follows: $R_{11} = R_{12} = 51$ kΩ, $R_{21} = R_{22} = 51$ kΩ, $R_{31} = R_{32} = 39$ kΩ, $R_{41} = R_{42} = 39$ kΩ, $R_{51} = R_{52} = 10$ kΩ, $R_{61} = R_{62} = 10$ kΩ, $R_{71} = R_{72} = 90$ kΩ, $C_1 = C_2 = 100$ nF, $C_{1m} = C_{2m} = 330$ nF, $v_{s1} = v_{s2} = -15$ V. Based on the parameter configuration, the variation rates α_1 for MC1 and α_2 for MC2 are both equal to 16.59 μF/Wb, and the initial MCA values of β_1 for MC1 and β_2 for MC2 are equal to 1.269 μF. The excitation voltage v_{12} can be characterized by a sinusoidal voltage $1.9\sin(20\pi t)$ V. Two potentiometers R_{c1} and R_{c2} with 1-MΩ maximal value are used for smoothly adjusting the coupled coefficients. For the sake of verifying the consistency between experimental and simulation results, the experimental data are sampled by oscilloscope TDS20114 and then transferred into OriginPro8.0 software to draw the curves.

According to Eqs. (49) and (51), we can obtain that the coupling coefficient κ_1 is in proportion to the variation rate κ_2 with the coefficient of $R_{12}C_2R_{32}/(R_{11}R_{c2}C_1)$. Based on the above experimental parameter configuration, the coefficient can be calculated and equal to R_{32}/R_{c2}. The charge q passing through the MC can be measured by sampling the output voltage of AD633 according to Eq. (46b). Under the condition of $R_{c1} = 79$ kΩ and $R_{c2} = 78$ kΩ, the experimental data of voltage and charge relating to terminals A_1B_1, A_2B_2, and A_1A_2 are measured to draw the PHLs at $\kappa_1 = 0.5\alpha_2$ and $\kappa_2 = 0.49\alpha_1$ as shown in Fig. 24(a). It can be seen that all the three PHLs behaving as an inclined "8" are together passing through the origin, and the curves of v_1–v_{w1} and v_2–v_{w1} are closely coincided with each other. Obviously, this experimental PHL is in good agreement with the simulation result shown in Fig. 10(a), which also reflects that each of the two MCs can behave as individual MC and the coupled MC circuit can also be operated as individual MC even in serial connection coupled MC with opposite polarities. The MCAs C_{m1}, C_{m2}, and C_{m12} varying with terminal voltages at $\kappa_1 = 0.5\alpha_2$ and $\kappa_2 = 0.49\alpha_1$ are shown in Fig. 24(b), which demonstrates that C_{m2} and C_{m12} decrease while C_{m1} increases due to positive terminal voltage. Evidently, the curves of C_{m1}–v_1 and C_{m2}–v_2 are almost identical to each other, which is in good consistence with Fig. 24(a).

By setting $R_{s1} = 200$ kΩ, $R_{s2} = 100$ kΩ, and $R_{s3} = 200$ kΩ, two coupled MCs in serial connection with opposite

polarities are used to structure the RO circuit. $R_{c1} = 500$ kΩ and $R_{c2} = 78$ kΩ are adopted to verify the MCA characteristics of MC1 and MC2 as operated in the RO circuit, as well as the output performance of the RO. Two identical Zener diodes of 1N4739 are utilized to restrict the output voltage within the interval of $[-9.1, 9.1]$ V. For the special case of $\kappa_1 = 0.5\alpha_2$ and $\kappa_2 = 0.078\alpha_1$, the measured experimental results are displayed in Fig. 25, from which we can see that all the three PHL curves behave as an inclined "8" as shown in Fig. 25(a). Note that these three PHLs stably evolve but with non-smooth ends, which can be attributed to the square waveform of the output oscillation voltage of RO. The square output voltage leads to approximate triangle terminal voltage of the MCs as shown in Fig. 25(b).

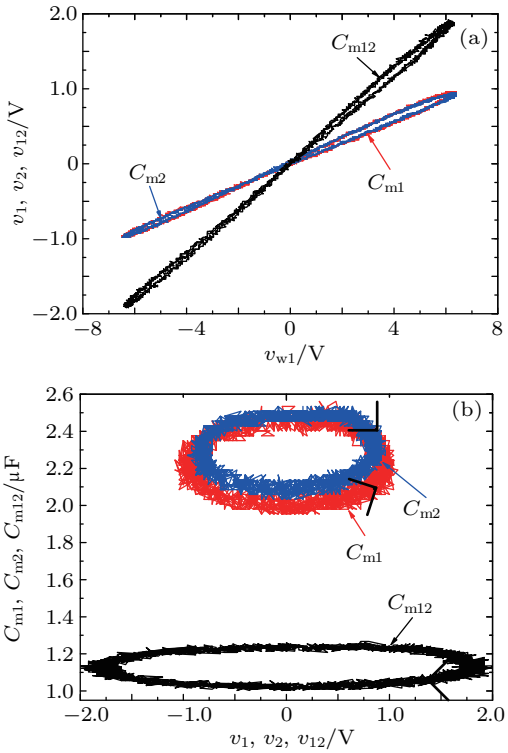


Fig. 24. (color online) Measured curves of two coupled MC circuits in serial connection. (a) PHLs; (b) MCA variation with terminal voltages at $\kappa_1 = 0.5\alpha_2$ and $\kappa_2 = 0.49\alpha_1$.

The MCAs varying with terminal voltage in the special case of $\kappa_1 = 0.5\alpha_2$, $\kappa_2 = 0.078\alpha_1$ are shown in Fig. 26(a), in which the MCAs C_{m2} and C_{m12} decrease while C_{m1} increases due to positive terminal voltage. The measured curves shown in Fig. 26(b) indicate that the coupled-MC-based RO can be self-excited and output square voltage waveforms with stable period and duty cycle. Meanwhile, by maintaining $R_{c2} =$ 79 kΩ leading to $\kappa_1 = 0.5\alpha_2$, four different cases with coupling coefficients of $\kappa_2 = 0.78\alpha_1$, $\kappa_2 = 0.5\alpha_1$, $\kappa_2 = 0.13\alpha_1$, and $\kappa_2 = 0.078\alpha_1$ are used to demonstrate the control effects of different coupling strengths on the output voltage of RO as shown in Fig. 26(b). It can be derived that with the increase of coupling coefficient κ_2, the duty cycle and the period of output voltage can both increase.

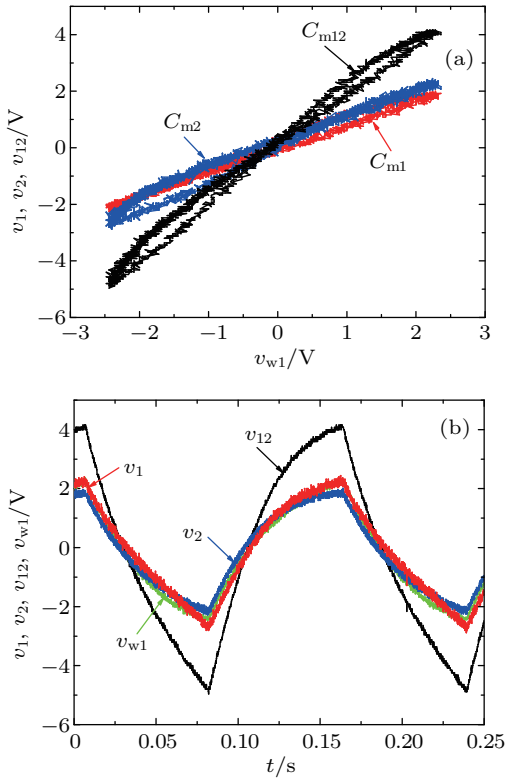


Fig. 25. (color online) Experimental results at $\kappa_1 = 0.5\alpha_2$, $\kappa_2 = 0.078\alpha_1$. (a) PHLs of MC1, MC2, and serial connection coupled MC; (b) Three terminal voltages and the output voltage of U61 in time domain.

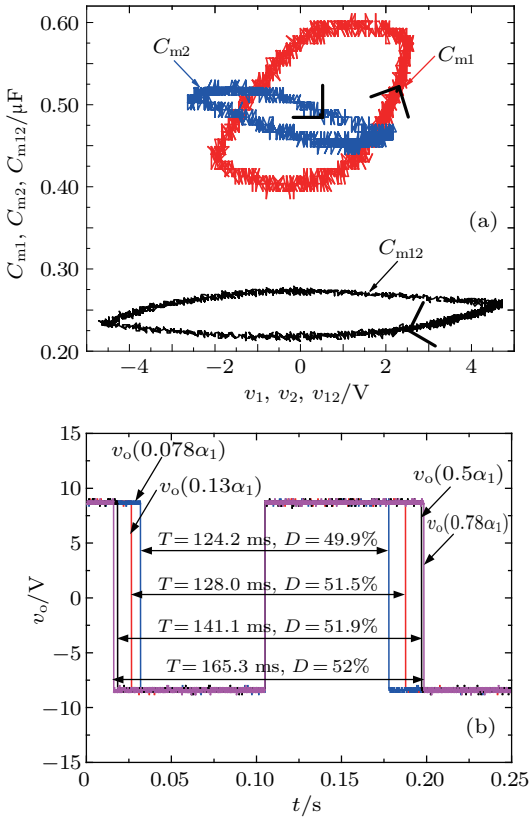


Fig. 26. (color online) Experimental results. (a) MCA varying with terminal voltages at $\kappa_1 = 0.5\alpha_2$, $\kappa_2 = 0.078\alpha_1$; (b) The output voltages of the RO under different values of coupling coefficient κ_2.

This dual coupled MC emulator can be connected in parallel with opposite polarities by linking A_1 with B_2, and

B_1 with A_2. The parameters for experimentally testing this parallel MC circuit are configured as $R_{11} = R_{12} = 51$ kΩ, $R_{21} = R_{22} = 51$ kΩ, $R_{31} = R_{32} = 39$ kΩ, $R_{41} = R_{41} = 39$ kΩ, $R_{51} = R_{52} = 10$ kΩ, $R_{61} = R_{62} = 10$ kΩ, $R_{71} = R_{72} = 90$ kΩ, $C_1 = C_2 = 100$ nF, $C_{1m} = C_{2m} = 220$ nF, $v_{s1} = v_{s2} = -15$ V. The variation rates α_1 and α_2 can be calculated and equal to 11.06 μF/Wb. The initial MCA value β_1 is the same as β_2, and both are equal to 0.8462 μF. The excitation voltage $v_{12} = 2\sin(20\pi t)$ V is employed for testing these MCs.

By maintaining the potentiometers $R_{c1} = 78$ kΩ and $R_{c2} = 800$ kΩ, we have $\kappa_1 = 0.78\alpha_2$ and $\kappa_2 = 0.5\alpha_1$. Based on Eq. (46b), v_{w1} is measured for representing the charge q_1 passing through MC1, while v_{w2} is measured for representing the charge q_2. The three PHLs of this dual coupled MC circuit in parallel connection with opposite polarities are shown in Fig. 27(a), where the PHLs with red, blue and black colors are the PHLs corresponding to MC1, MC2, and the MC circuit in parallel. The curves of MCAs varying with charges at $\kappa_1 = 0.049\alpha_2$ and $\kappa_2 = 0.5\alpha_1$ are given in Fig. 27(b). The measured MCA of the coupled MC circuit is equal to the sum of the MCAs of MC1 and MC2, hence it is possible that C_{m1} and C_{m12} increase while C_{m2} decreases for positive charge, as the curves are shown in Fig. 27(b).

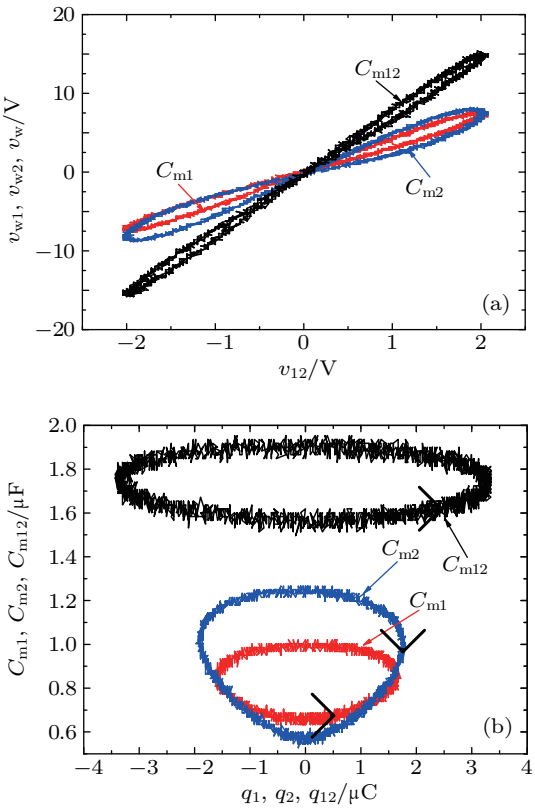


Fig. 27. (color online) Measured curves of two coupled MC circuits in parallel connection with opposite polarities. (a) PHLs; (b) MCA variation with charge at $\kappa_1 = 0.049\alpha_2$ and $\kappa_2 = 0.5\alpha_1$.

The curves of C_{m12} varying with flux φ_{12} are displayed in Fig. 28, in which the coupling coefficient $\kappa_2 = 0.5\alpha_1$ and the coupling coefficient κ_1 changes from $0.078\alpha_2$ to $2.5\alpha_2$. It can be observed that the MCA can be linearly reduced by the increase of the flux as κ_1 is greater than $0.5\alpha_2$, while the MCA can linearly increase with increasing flux as κ_1 is less than $0.5\alpha_2$. For the special case of $\kappa_1 = 0.5\alpha_2$, the MCA remains constantly equal to its initial value of 1.74 μF no matter whether the flux is varying.

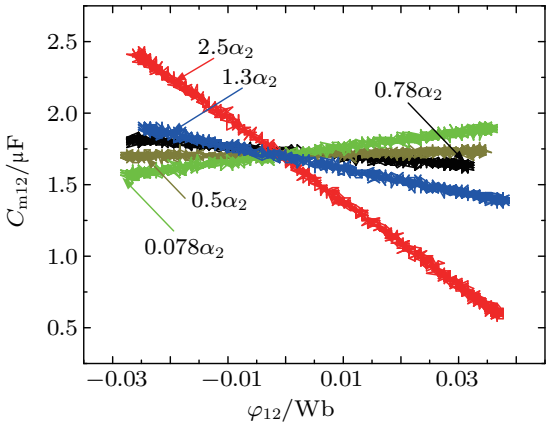


Fig. 28. (color online) Measured curves of MCA varying with flux under different values of coupling coefficient κ_1.

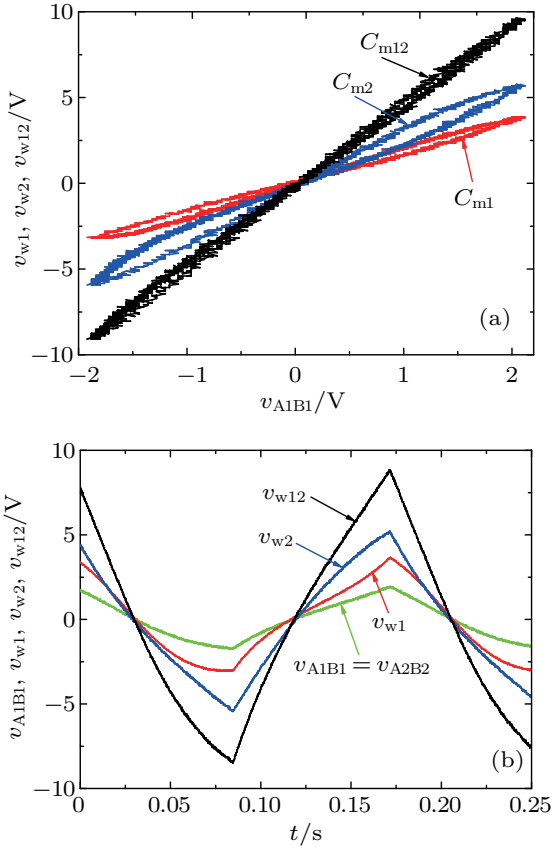


Fig. 29. (color online) Experimental results at $\kappa_1 = 3.9\alpha_2$ and $\kappa_2 = 0.5\alpha_1$. (a) PHLs of MC1, MC2, and the coupled MC circuit; (b) three terminal voltages and the output voltage of U61 in time domain.

The parameters for implementing the RO with coupled MCs in the parallel connection are configured as $R_{s1} = 200$ kΩ, $R_{s2} = 100$ kΩ, and $R_{s3} = 23$ kΩ. By setting $R_{c1} = 78$ kΩ and $R_{c2} = 10$ kΩ, it can be calculated that coupling strengths satisfy the condition of $\kappa_1 > \kappa_2$. The experimental curves are displayed in Fig. 29(a), from which we can

see that the PHLs of MC1, MC2 and the coupled MC circuit are together passing through the origin but with very different shapes and variation rates. Hence, it can be speculated that the variation of MCA with terminal voltage across each MC is also different from the other MC due to the influence from coupling strength. Three terminal voltages and the output voltage of U61 in time domain are shown in Fig. 29(b) for comparative exhibition.

By keeping $R_{c1} = 78$ kΩ and $R_{c2} = 10$ kΩ, we can calculate that the coupling coefficients $\kappa_1 = 3.9\alpha_2$ and $\kappa_2 = 0.5\alpha_1$. Three curves of MCA versus charge are displayed in Fig. 30(a), in which the MCA of the coupled MC circuit is equal to the sum of the MCAs of MC1 and MC2. Obviously, the MCAs of C_{m1} and C_{m12} can increase while C_{m2} decreases by positive terminal voltage. Shown in Fig. 30(b) are the three output voltages under different values of coupling coefficient κ_1 and a fixed value of coupling coefficient κ_2. It can be concluded that with the increase of coupling coefficient κ_1, the duty cycle and the period of output voltage both increase.

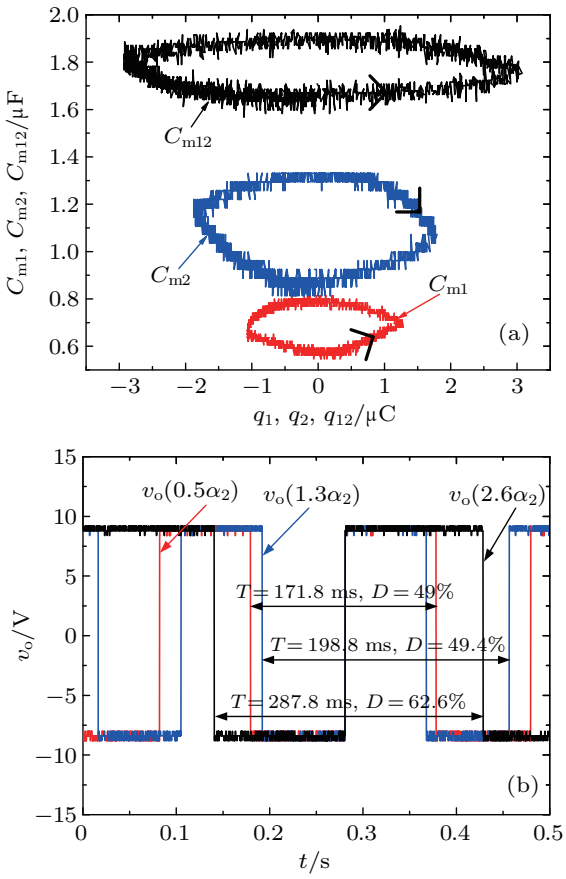


Fig. 30. (color online) Experimental results. (a) MCA varying with charge at $\kappa_1 = 3.9\alpha_2$, $\kappa_2 = 0.5\alpha_1$; (b) output voltages of the RO under different values of coupling coefficient κ_1.

In order to verify the controllability of different coupling strengths, $\kappa_1 = 0.5\alpha_2$ and κ_2 varying from 0 to α_1 are adopted to carry out the experimental validation for the case of the serial connection as shown in Fig. 31(a), while the parameter configuration of $\kappa_2 = 0.5\alpha_1$ and κ_1 varying from 0 to $2.6\alpha_2$ are employed for the experimental implementation for the case of parallel connection as shown in Fig. 31(b). Clearly, the high coupling coefficients κ_1 and κ_2 can lead to high oscillation periods and duty cycles. As shown in Fig. 31(a), the variation ranges of oscillation duty cycle and period are [49.2%, 52.5%] and [120.9, 170] ms, respectively. Meanwhile, the variation ranges of oscillation duty cycle and period are measured to be [48%, 59%] and [160.2, 270.3] ms, respectively, as depicted in Fig. 31(b).

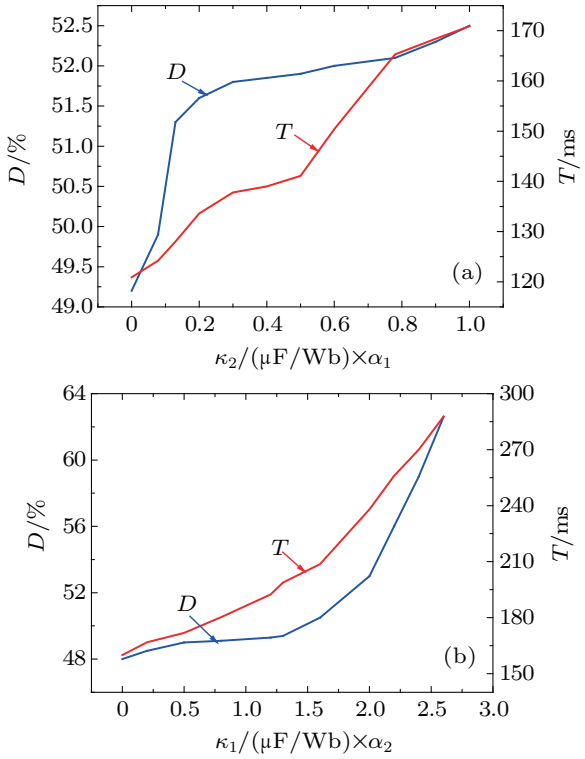


Fig. 31. (color online) Experimental results of controllability. (a) Serial connection; (b) parallel connection.

These experimental results show that the proposed emulator circuit is capable of mimicking the dynamic behaviors of coupled MCs. At the same time, the coupled MC with multiple circuitry connections can be used to structure the RO with adjustable period and duty cycles. These experimental results exhibit good agreement with the theoretical and simulation results.

8. Conclusions

The dynamic behaviors of two flux-coupled MCs are comprehensively discussed based on the chosen specific constitutive relations. The simulation and experimental results of coupled MC circuit reflect that the dynamic characteristics of two coupled MR circuits highly depend on the coupling strength and connection polarities. The coupled MC circuits are then used for designing new RO with the expected adjustments of oscillation period and duty cycle. The simulation and experimental results show that the output frequency and

duty cycle of the RO are nonlinearly dependent on parameters of the coupled MCs. Hence, the controllable coupling potentiometers need properly configuring in order to obtain the required output duty cycle and frequency with high accuracy. By taking advantage of the coupling action, the oscillation period and duty cycle of the coupled-MC-based RO both can be controlled on purpose, which shows the potential applications of the coupled MC in electrical circuit for the sake of good controllability and practicability. By tuning the coupling coefficients, the oscillation period and duty cycle can be purposefully controlled.

References

[1] Chua L O 1971 *IEEE Trans. Circ. Th.* **18** 507
[2] Di Ventra M, Pershin Y V and Chua L O 2009 *Proc. IEEE* **97** 1717
[3] Bao B C, Yu J J, Hu F W and Liu Z 2014 *Int. J. Bifur. Chaos* **24** 1450143
[4] Yu Q, Bao B C, Hu F W, Xu Q, Chen M and Wang J 2014 *Acta Phys. Sin.* **63** 240505 (in Chinese)
[5] Wu H G, Bao B C and Chen M 2014 *Chin. Phys. B* **23** 118401
[6] Wang G Y, Cai B Z and Jin P P 2016 *Chin. Phys. B* **25** 010503
[7] Pershin Y V and Ventra M D 2012 *Proc. IEEE* **100** 2071
[8] Li C B, Li C D and Huang T G 2013 *Neurocomputing* **12** 370
[9] Pei J S, Wright J P, Todd M D, Masri S F and Gay-Balmaz F 2015 *Nonlinear Dyn.* **80** 457
[10] Driscoll T, Quinn J, Klein S, Kim H T, Kim B J, Pershin Y V, Di Ventra M and Basov D N 2010 *Appl. Phys. Lett.* **97** 093502
[11] Wang G Y, Cai B Z, Jin P P and Hu T L 2016 *Chin. Phys. B* **25** 010503
[12] Yu D S, Liang Y, Iu H H C and Chua L O 2014 *IEEE Trans. Circuits and Sys. II, Exp. Briefs* **61** 758
[13] Yu D S, Liang Y, Iu H H C and Hu Y H 2014 *Chin. Phys. B* **23** 070702
[14] Biolek D, Biolek Z and Biolkova V 2010 *Electron. Lett.* **46** 520
[15] Yu D S, Liang Y, Chen H and Iu H H C 2013 *IEEE Trans. Circuits and Sys. II, Exp. Briefs* **60** 207
[16] Biolek D, Biolkova V, Kolka Z and Dobes J 2016 *Circ. Sys. Signal. Pr.* **35** 43
[17] Fouda M E, Khatib M A and Radwan A G 2013 *25th International Conference on Microelectronics (ICM)*, December 15–18, 2013, Beirut, Lebanon, p. 1
[18] Sah M P, Budhathoki R K, Yang C and Kim H 2013 *Int. J. Bifur. Chaos* **23** 1330017
[19] Fouda M E and Radwan A G 2015 *Circ. Sys. Signal. Pr.* **34** 2765
[20] Fouda M E and Radwan A G 2015 *Int. J. Circ. Theor. Appl.* **43** 959
[21] Yuan F, Wang G Y and Wang X W 2017 *Chaos* **27** 033103
[22] Wang G Y, Zang S C, Wang X Y, Yuan F and Iu H H C 2017 *Chaos* **27** 013110
[23] Wang G Y, Shi C B, Wang X W and Yuan F 2017 *Math. Probl. Eng.* **2017** 6504969
[24] Cai W R and Tetzlaff R 2014 *IEEE International Symposium on Circuits and Systems (ISCAS)*, June 1–5, 2014, Melbourne, Australia, p. 1259
[25] Yu D S, Zhou Z, Iu H H C, Fernando T and Hu Y 2016 *IEEE Trans. Circuits and Sys. II, Exp. Briefs* **63** 1101